AN ASSESSMENT OF COASTAL EROSION IN THE MINAS BASIN, NOVA SCOTIA

by

Erin Wilson

Submitted in partial fulfillment of the requirements
for the degree of Master of Science

at

Dalhousie University
Halifax, Nova Scotia
July 2016

In every outthrust headland, in every curving beach, in every grain of sand there is the story of the earth

-Rachel Carson

TABLE OF CONTENTS

LIST OF TABLES

LIST OF FIGURES

ABSTRACT

Understanding sediment processes in the Minas Basin, Nova Scotia, is essential for determining the potential impacts tidal power extraction could have on the system. The main source of sediment to the Minas Basin is the eroding coastline, which is dominated by sandstone cliffs. This thesis uses Geographic Information System methods to generate highly resolved measurements of the locations and volumes of sediment input. Inputs from coastal sources have increased from 9.0 x 10^5 to 1.3 x 10^6 m^3/yr since the 1960s, as erosion rates have increased along most of the coastline. The largest sediment source is the northern shore of the Central Basin, from Five Islands to Parrsboro. The amount of sediment entering the Minas Basin is enough to overwhelm the systems ability to remove it, suggesting that changes in sediment bed texture cannot be predicted from changes in bottom current speeds alone.

List of Abbreviations and Symbols Used

Abbreviation/Symbol	Description
m	metre
km	kilometre
m/yr	metres per year
mm/yr	millimetres per year
m^3/yr	cubic metres per year
$m^3/yr/m$	cubic metres per year per metre
g/cm^3	grams per cubic centimetre
mg/L	milligrams per litre
%	percent
°	degree
S.D.	Standard Deviation
GIS	Geographic Information System
GPS	Global Positioning System
LiDAR	Light Detection and Ranging
AMBUR	Analysing Moving Boundaries Using R
DEM	Digital Elevation Model
TIN	Triangulated Irregular Network
NSTDB	Nova Scotia Topographic Database
UTM	Universal Transverse Mercator
ANOVA	Analysis of Variance
TOPO	Topographic
NAD83	North American Datum of 1983

ACKNOWLEDGEMENTS

Firstly, I would like to thank my supervisor, Paul Hill for his advice and guidance throughout this process. A huge thank you to Stephanie Kienast for all of her support and encouragement throughout my years at Dalhousie. Thank you also to Danika van Proosdij for all her help with GIS, development of methods and guidance throughout writing my thesis. I would like to acknowledge NSERC for providing funding for this project. Thank you to Markus Kienast, Helmuth Thomas, and the Department of Oceanography for providing opportunities outside of my research to spend time at sea and explore other areas of ocean science. To DOSA, thank you for making these past years so fun, I couldn't ask for better people to share this experience with. Lastly, to all of my family and friends for following me on this journey; I am eternally grateful for your love and support.

CHAPTER 1

INTRODUCTION

The Minas Basin, Nova Scotia is home to the world's highest tides and a dynamic coastline. Mean tidal range is 12 m with a maximum reaching 16.3 m at Burntcoat Head (*Parker et al.*, 2007; *Desplanque and Mossman*, 2004). Current speeds in the Minas Channel can reach 8 knots, and the tide carries nearly 3 billion cubic meters of water in and out of the Basin with each tidal cycle (*Parker et al.*, 2007). Due to these fast currents and the immense amount of energy present in the system, the area has long been of interest for tidal power generation (*Li et al.*, 2013). Most recently, testing has begun for the placement of large in-stream tidal turbines in the Minas Channel. Emplacement of tidal turbines could have an affect on currents as energy is being extracted and, therefore, could affect grain size distributions in this system. To fully understand the changes that harnessing tidal power could cause, a baseline of present day conditions needs to be established, including an updated sediment budget. The first element of that is an updated study of the major sediment source to the Basin, which is coastline erosion (*Amos and Long*, 1980).

1.1 The Minas Basin

The Bay of Fundy extends to the northeast from the Gulf of Maine and splits into two inner basins, the Chignecto Bay to the north and the Minas Basin to the south. The Minas Basin is a semi-enclosed macrotidal embayment and can be divided into four sections (Figure 1.1): The Minas Channel, which connects the Minas Basin to the outer Bay of Fundy, the Central Minas Basin, extending between Cape Split and Economy, the Southern Bight,

the southern most section of the Basin, and the Cobequid Bay, the eastern most section extending from Economy to the mouth of the Salmon River. This study focuses on the Central Minas Basin, the Cobequid Bay and the Southern Bight. These three sections together create an almost triangular bay with a length of 62 km and a maximum width of 26 km (*Parker et al.*, 2007). The high tides in this system result because the natural period of oscillation of the Bay of Fundy nearly matches the tidal period, resulting in resonance (*Garrett*, 1972). The Minas Basin is relatively sheltered from swells in the outer Bay of Fundy by Cape Split; therefore, the waves in the Minas Basin are mostly locally wind generated (*Amos and Long*, 1980; *Parker et al.*, 2007).

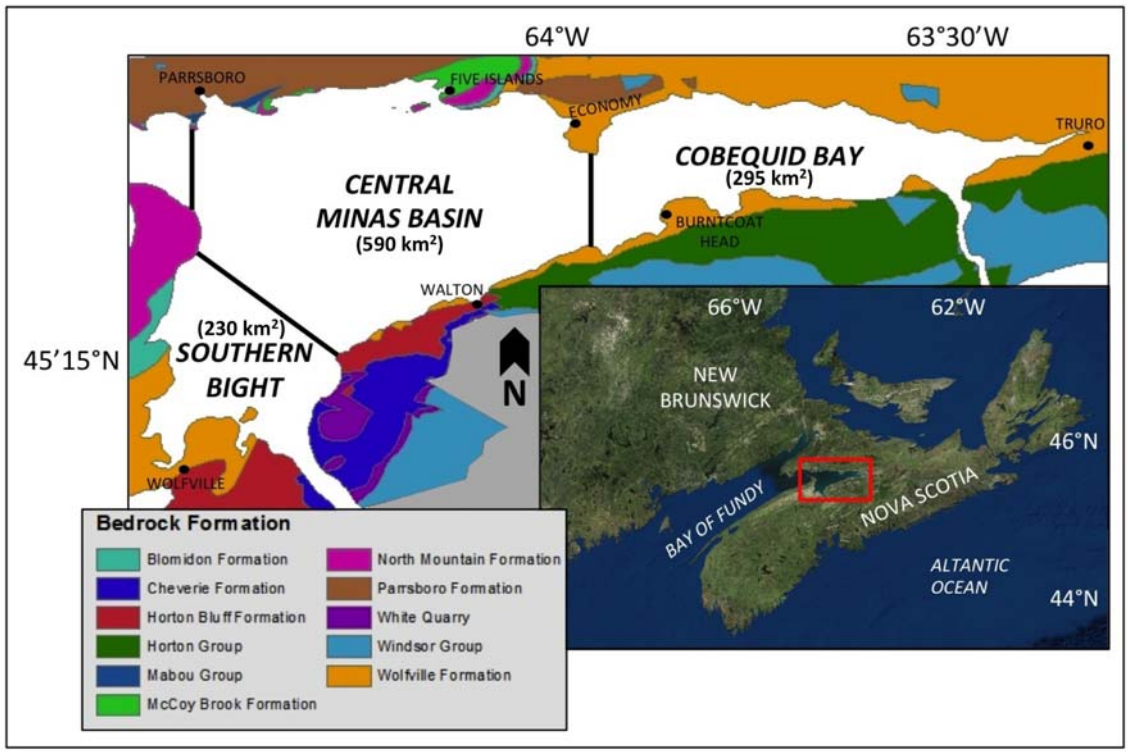

Figure 1.1: Minas Basin study area with surrounding bedrock formations. Bedrock geology data from the NSTDB 1:10 000 maps property of Service Nova Scotia.

1.1.1 Geology

The Minas Basin was formed in the Early Mesozoic during the early rifting stages of Pangaea. Throughout early development of the basin, Upper Triassic and Lower Jurassic

sediments were deposited (*Kettanah et al.*, 2013).

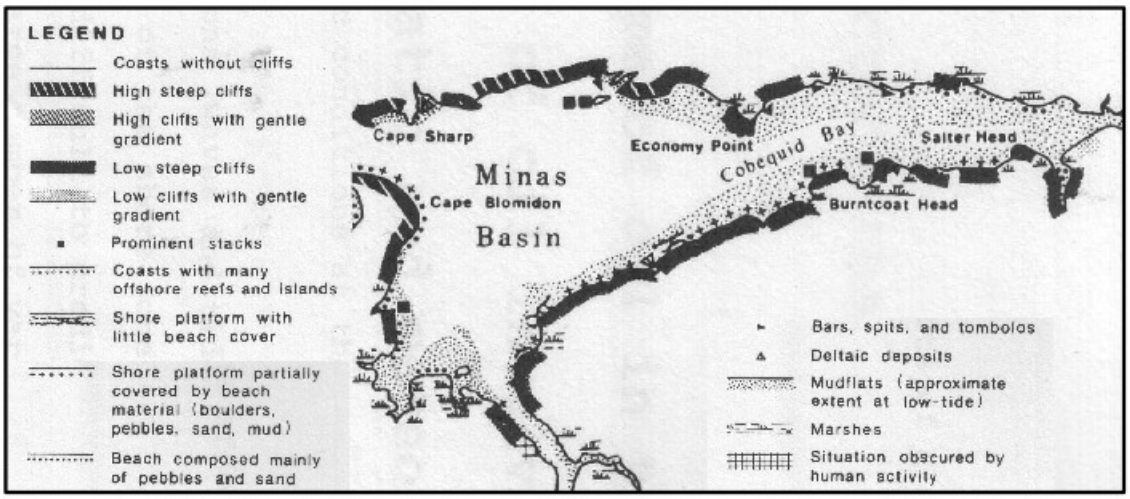

Figure 1.2: Coastal morphology of the Minas Basin adapted from *Owens* (1977).

Today, the Minas Basin is predominantly surrounded by steep cliffs that bound 79% of the perimeter. These cliffs are made up of unstable Triassic sandstone along with Cretaceous Basalt, Paleozoic sedimentary rocks, and Quaternary glacial till and outwash (*Amos and Long*, 1980). The highest steep cliffs lie along the north shore of the Central Minas Basin, between Parrsboro and Five Islands as well as along Cape Split. Lower steep cliffs dominate the rest of the northern shore of the Central Basin as well as the southern shore of the Central Basin and Cobequid Bay (Figure 1.2).

The Wolfville formation is the bedrock formation that is exposed along a majority of the coastline (Figure 1.1). It is composed of sediments deposited during continental rifting (*Kettanah et al.*, 2013). Quartz is the dominant mineral and grain-size within the Wolfville formation ranges from fine to coarse. Porosity ranges from 1 to 17% and is shown to be both primary and secondary (*Kettanah et al.*, 2013). The red colour of many of the cliffs in the region is due to the presence of iron-rich hematite, which is oxidized easily (*Parker et al.*, 2007).

1.2 Cliff Erosion

Sea cliffs are steep slopes that border the ocean. They occur on almost 80% of the global coastline (*Emery and Kuhn*, 1982). The processes that cause cliff erosion are split into two categories, marine and terrestrial processes (*Benumof and Griggs*, 1999; *Emery and Kuhn*, 1982; *Pye and Blott*, 2015). Anthropogenic interference has also become a major cause of coastal erosion in the form of coastal infrastructure and dredging (*Martinez et al.*, 2014).

Terrestrial processes of cliff erosion include rainwash, gullying, and frost wedging (*Emery and Kuhn*, 1982). The resistance of the cliff material also can affect the erosion rate. Often, rock hardness and the geology of a cliff play a role in determining erosion rates (*Benumof and Griggs*, 1999). Cliff composition is capable of affecting the shape of coastline, where homogeneous composition of either resistant or non-resistant material will lead to more even erosion and sloped cliffs give clues to a more heterogeneous composition (*Emery and Kuhn*, 1982). As slope gradient increases the sediment flux down the slope face is known to increase (*Dietrich et al.*, 2013; *Larinov et al.*, 2015). *Young et al.* (2009) noted in a study in Southern California that most sea cliff failures were triggered by rainfall and groundwater seepage but were accelerated by wave attack at the base of the cliff. Chemical properties also become important on limestone coasts (*Sunamura*, 1977).

Wave attack is one of the more dominant marine processes that affects cliff erosion. Solution from ocean water, biological activity, and water level can also play a role (*Revell et al.*, 2011). Wedge action caused by wave energy compressing air in fissures within the rock can also aid in erosion (*Longwell et al.*, 1969). *Lim et al.* (2011) note that when wind and waves propagate along the direction of maximum fetch at high tide, critical tide levels exist. At these critical tide levels, more energy is delivered to the cliff foot, and increased erosion can occur. Even though the effects of tides and waves on coastal erosion are well recognized, the connection between these two forces and other environmental variables are still poorly understood (*Lim et al.*, 2011).

Suspended sediment near cliff faces also is known to cause increased erosion. This affect arises because the grains act as an abrasive tool and aid in erosion processes (*Bird*, 1969; *Pye and Blott*, 2015; *Robinson*, 1977). *Robinson* (1977) noted that erosion rates along the Yorkshire coast in England were 15 - 18.5 times higher when there was a beach

source of suspended sediment in front of the cliff. Other debris in the water, like ice and wood, can have a similar effect. Ice cover can help dampen wave effects in the winter months, but can also cause undercutting and abrasion (*O'Carroll*, 2010).

Sunamura (1977) found that the erosion rate ($\frac{dX}{dt}$) of a cliff is proportional to the erosive force of waves (F) (Equation 1.1). The erosive force of the waves will cause the cliff to erode when the assailing forces (f_w) are greater than the resisting forces (f_r) (Equation 1.2).

$$\frac{dX}{dt} \propto F \tag{1.1}$$

$$F = \ln(\frac{f_w}{f_r}) \tag{1.2}$$

Assailing forces include hydraulic actions, such as compression, tension and wear, as well as weathering, fatigue, and abrasive action. Resisting forces include mechanical properties, compressive and tensile strength, and structure, such as joints, faults and stratification (*Sunamura*, 1977).

As erosion increases from marine processes, mass movement by rock falls and slumps is more common as the cliffs become undercut (*Emery and Kuhn*, 1982). Cliffs made of hard rock on the North Yorkshire coast showed that failure mechanisms drove erosion. However, the relationship between cliff inundation and energy transfer from the ocean and along the coast is complex, so simple tidal inundation models generally do not explain variations in erosion rates (*Vann Jones et al.*, 2015). A greater understanding of cliff behaviour is critically important especially given the threat of global sea-level rise (*Lim et al.*, 2011).

1.3 Previous Sediment Budget

A sediment budget was completed for the Minas Basin, Nova Scotia by *Amos and Long* (1980). The budget was assessed in terms of the present sediment characteristics of the basin: inputs from cliffs, rivers and open sea and losses to open sea. The sources were added and the losses subtracted to determine the net sediment accumulation or erosion in the Basin (*Amos and Long*, 1980).

This sediment budget determined that the dominant input of sediment to the Minas Basin system was from cliff erosion, providing sediment of mostly sand-sized grains. Rough estimates of volumetric inputs from the cliff sources are 3.09 x 10^6 m^3/yr (*Amos and Long*, 1980). These were completed by measuring cliff height stereoscopically from aerial photographs in 158 locations. These measurements were checked through field measurements at an undisclosed number of sites and methods were not stated. River inputs were also assessed, but it was determined that the majority of sediment entering the system was derived from the bordering cliffs (*Amos and Long*, 1980).

Cliff erosion rates were determined for this sediment budget, but the measurements were not continuous along the entire coastline. Eighteen sections were given erosion rates based on 105 sites assessed around the basin from aerial photographs taken from 1939 - 1964. The rates were based on the mean of four independent measures (*Amos and Long*, 1980), however, the method used for completing this measurement was not specified. They found a mean erosion rate of 0.55 m/yr with maximum rates of 1.5 m/yr at Five Islands and 1.6 m/yr along the north shore of Cobequid Bay. They stated that rates were lower, with a mean of 0.5 m/yr, along the southern shore of the Minas Basin with no noticeable erosion measured at Burntcoat Head.

Sediment input in the Basin has been increasing in postglacial times, with the proportion of finer material decreasing as tidal strength has increased. However, *Amos and Long* (1980) also observed, based on tidal innundation of the current wave platform and assuming that cliff heights have remained the same, that cliff erosion rates have remained largely constant over the past 4900 years.

Suspended sediment concentrations range from 1 mg/L to 2700 mg/L in the Basin

(*Amos and Long*, 1980) with concentrations increasing towards the head of Cobequid Bay. Movement within the Bay of this material is dominated by residual tidal currents but may be influenced by other currents closer to shore (*Amos and Long*, 1980). These currents carry sediment eastward into Cobequid Bay and southward into Windsor Bay. *Amos and Long* (1980) also observed eastward migration of sand using radioisotope dating in the intertidal zone at Economy point at a rate of 0.46 x 10^6 m^3/yr. Sand found on the seafloor along the north shore and in Cobequid Bay appears to have originated near Five Islands. Net accretion of sediment in Cobequid Bay is thought to be equivalent to all of the sediment derived from cliff erosion along the north shore of the Central Basin (*Amos and Long*, 1980), showing the majority of eroded sediment remains within the Minas Basin system. *Amos and Long* (1980) conclude, by looking at basin volume increase from sea level rise and erosion compared with the volume of sediment added each year, that the Minas Basin system is decreasing in volume at a rate of 1.4 x 10^6 m^3/yr.

When seabed texture and near-bed flow are in equilibrium, it is relatively simple to predict changes in grain size based on changes in flow. Previously, sediment dynamics and transport rates in the Bay of Fundy had been described based on equilibrium in the system (*Emery and Uchupi*, 1972; *Amos and Long*, 1980). However, *Gelati* (2012) showed that sediment texture in the Bay of Fundy is generally out of equilibrium with the maximum tidal bed shear stress. The expected bed grain size based on maximum near bed flow is larger than what is actually observed. With such strong currents in the system, it was expected that there would be a strong correlation between near bed flow and sediment texture because suspended sediment would be carried away. *Gelati* (2012) suggested that sediment supply could be the cause of this departure from equilibrium. Large inputs of sediment finer than competent observed grain size can cause bed grain size to be finer than expected (*Buffington and Montgomery*, 1999). A recent study by *Li et al.* (2015) modeled sediment transport in the Bay of Fundy and found models accurately showed directions of net flux, but the amount of sediment being transported was an order of magnitude smaller than observed. In order to better be able to model the sediment dynamics in the Minas Basin, the input of sediment to the system, predominantly from cliff erosion, needs to be better constrained.

1.4 Significance of Study

A report put forward by the Atlantic Geoscience Society in 2006 noted that research in this area had been scant since the 1970's and 1980's when initial investigation into tidal power implementation began. The report stressed that a better understanding of the geologic, physical and biological processes in the region is needed to make the best management decisions, especially with the rate of coastal erosion, the continued push for tidal power implementation, and the observed increase in tidal range (*Butler et al.*, 2006). One recommendation for research was the development of a new sediment budget for the Bay of Fundy. This project aims to quantify the amount of sediment entering the Minas Basin from coastal erosion in order to contribute to an updated sediment budget for the area.

Tidal range in the Minas Basin has increased throughout the Holocene. The present day sea level is increasing at a rate of 3.0 mm/yr as measured by tide gauges since the 1930's. Eustatic global sea level rise is amplified in this area by crustal subsidence due to the retreat of ice from the last glacial maximum (*Gehrels et al.*, 2004). This increase in sea level, coupled with the prediction of increased storminess (*Jones et al.*, 2007) and the implementation of in-stream tidal turbines, further stresses the need for fuller understanding of the dynamics of this coastline and the areas that are most at risk.

More accurate and detailed measurements of sediment inputs to this system also have implications for understanding grain size in the Basin. Sediment texture is important for benthic plants and animals (*Methratta and Link*, 2006) and tidal power is expected to cause sediment fining in some areas of the Minas Basin and coarsening in others (*Gelati*, 2012).

In the Minas Basin, it is likely that the tides dominate sediment transport but do not dominate sediment texture, as there are large inputs from the surrounding sandstone cliffs (*Gelati*, 2012). *Li* (2011) stresses the need to better understand present-day sediment dynamics before an impact assessment on tidal power can be completed. Also, future models of sediment texture must include supply from coastal erosion to accurately show the current state of the system (*Gelati*, 2012). By creating a clear picture of the baseline state of the system, potential affects of harnessing tidal power can be better predicted.

1.5 Objectives

The objectives of this thesis are (1) to provide highly resolved measurements of erosion rate along the Minas Basin coastline using aerial photographs and GIS techniques (2) to combine erosion measurements with digital elevation models to accurately estimate the amount of sediment entering the Minas Basin from coastal sources and (3) to assess possible causes for variations in erosion rates around the Basin which could be used to focus mitigation efforts or plan infrastructure. By providing updated measurements of the largest sediment source to the Minas Basin system, this study will provide essential data for creating an updated sediment budget as well as provide detailed spatial resolution of sediment entering this system that can be used in future models of sediment texture and transport in the Basin. This information is crucial in providing a baseline picture of conditions in the Minas Basin before the inplementation of in-stream tidal turbines.

CHAPTER 2

METHODOLOGY

2.1 Methods in Erosion Analysis - Literature Review

Previous studies of coastal erosion in the Minas Basin were limited in the resolution that could be achieved. Although aerial photographs were available, calculated erosion rates and volumetric inputs along the coastline were computed at discrete points. Values from those widely space discrete sites were used to represent a long stretch of coastline. With Geographic Information Systems (GIS), software designed to work with and display geographically referenced data, more accurate and higher resolution measurements are possible.

2.1.1 Defining the Coastline

When assessing the coastal erosion in any given area, defining the shoreline is an essential step. A clear and constant definition of the shoreline must be used when assessing shoreline changes because the environments being studied are often very dynamic. *Boak and Turner* (2005) provide examples of shoreline indicators that can be used when assessing changes to coastal environments. They stress that it is important to consider the appropriate time scales of observations. For example, an instantaneous shoreline may not represent the average or normal shoreline for that area. If a shoreline is looked at on tidal cycle scale, there can be variations of cm to m (*Boak and Turner*, 2005). A shoreline indicator, or a feature that is used as a representation of the actual shoreline position, is often used

when assessing coastal environments. Shoreline indicators can be determined from a visually apparent feature on the coastline, such as a wet/dry boundary, or can be based on a specific tidal datum, such as a mean high water line (*Boak and Turner*, 2005). Other indices include: cliff/bluff top, base of cliff/bluff, seaward dune vegetation line, storm debris line and various water line indicators. Bluff or cliff lines as well as dune lines are good indicators of erosion, but will not show accretion as clearly (*Moore et al.*, 1999; *Stafford and Langfelder*, 1971).

2.1.2 Data Sources

Several data sources can be used to determine shoreline positions as well as their changes. The limiting factor is often the availability of data in the area of interest. Multiple types of data are often used simultaneously for any given assessment (*Boak and Turner*, 2005).

Photographs are one common data source. These can be in the form of land based or aerial. Land based historical photography is often used more for background information on scale, tides or control points (*Dolan et al.*, 1983). Temporal resolution of shoreline imagery varies from site to site and must be considered. When evaluating long term shoreline changes, decade scale resolution is adequate (*Boak and Turner*, 2005).

Other data sources include coastal maps and charts, which became more reliable in the 18th century (*Carr*, 1962), as well as more modern techniques such as GPS mapped coastlines (*Morton et al.*, 1993), beach surveys, remote sensing and LiDAR (Light Detection And Ranging) (*Boak and Turner*, 2005; *Brock and Purkis*, 2005). LiDAR uses light from a laser to measure distances and create high resolution maps of both man-made and natural features. Detecting the identified shoreline within the chosen data source is usually completed by manual visual interpretation and relies on the individual doing the assessment (*Dolan et al.*, 1983). Familiarity with the study area and indentification of shoreline features in the field greatly increases the accuracy of shoreline detection from aerial photographs (*Byrnes et al.*, 1991).

2.1.3 Erosion Measurement Methodology

Often, the techniques used for measuring coastline change, as well as the definition used for the coastline itself, are chosen based on the reason for measuring that change. Monitoring

Table 2.1: Error associated with methods in measuring coastal erosion

	Methods	Associated Error
Direct	GPS Field Measuements	mm - cm
	Tape Measure Field Measurements	<2 m
Indirect	Digital Photogrammetry	2 - 7 m
	Zoom Transfer Scope	10 m
	Cadastral Maps	10 m

projects and assessment of seasonal changes require short-term observations. Assessments of longer term changes are more useful for planning and measuring long-term trends (*Raju et al.*, 2010). Repeat surveys carried out four times a year along fixed profile lines from a marker to a designated waterline is one technique discussed by *Raju et al.* (2010) for measuring short to medium term changes. Errors associated with field measurements are generally mm to cm using a GPS and no more than 2 m using a tape measure (*O'Carroll*, 2010). Overlaying aerial photographs or topographic maps is a method used for assessing longer term changes as long as distortions in the photographs are corrected (*Raju et al.*, 2010).

For longer time scale analysis, indirect measurements are often completed on maps, aerial photographs and satellite images. These measurements can be done using GIS with accuracy of a few meters. GIS methods using aerial photography are the most accurate indirect methods to measure historical erosion rates (*O'Carroll*, 2010). Older methods such as using a Zoom Transfer Scope or Cadastral maps have accuracies up to 10 meters (*O'Carroll*, 2010).

Using GIS for assessing coastline erosion has become a widely used technique. GIS is a helpful tool in assessing shoreline change because it can be used in many ways. One of the advantages is being able to distinguish and classify different types of coastlines (*Davis*, 2011). It is also commonly used to assess long term coastline variation as the error associated with using aerial photograph comparisons can be too high to be used for short term changes in high water lines (*Armaroli et al.*, 2006).

Models can be created using GIS to assess changes in coastline. The AMBUR (Analysing Moving Boundaries Using R) model uses transect and baseline techniques to

measure changes from a set baseline offshore to the shoreline. There is also an option to project future shoreline changes, which sets it apart from other erosion assessment models (*Jackson et al.*, 2012). *Chaaban et al.* (2012) used a similar method using Modelbuilder in ArcGIS to measure changes in distance from transects to coastlines from aerial photographs over 59 years on coastlines in Northen France. The models measure the distances from the transects to the coastlines at chosen points and add the values to an attribute table (*Chaaban et al.*, 2012).

2.1.4 Volumetric Measurement Methodology

Digital Elevation Models (DEMs) are the most common tool used when assessing volumetric sediment losses along a coastline. DEMs from LiDAR data provide highly accurate and detailed elevation data (*Woolard and Colby*, 2002). Raster models are often more appropriate when working with DEMs, but triangulated irregular networks (TINs) allow for elevation to be represented with vector models (*Raju et al.*, 2010; *Woolard and Colby*, 2002).

In areas where DEMs are available from different time periods, they can be compared to assess changes in elevation and therefore volumetric sediment changes. This has been done using an ERDAS Imagine software package with a Spatial Modeler function that can difference two DEMs with the same extent, grid size and referencing system giving both positive and negative elevation changes (*Woolard and Colby*, 2002). Similarly, the *Minus Tool* in ArcGIS *Spatial Analyst* can be used to subtract elevations and the *Cut/Fill* tool can produce a raster showing areas where material was added, removed or did not change (*Pepe and Coutu*, 2008).

There are multiple techniques and methods to identify and assess physical changes to coastlines. The best approach for any given assessment should be based on the type of coastline being assessed, the time-scale on which the changes are being evaluated and the reason for completing the measurements. Quantifying shoreline changes and erosion is also an important aspect of creating sediment budgets for coastal regions.

2.2 Data Information

All aerial photographs for this study were obtained from the Province of Nova Scotia Aerial Photography Library and are available through the Nova Scotia Geomatics Centre Data Locator. LiDAR DEM data samples were provided by Dr. Tim Webster from the Applied Geomatics Research Centre at the Centre of Geographic Sciences at the Nova Scotia Community College. Nova Scota topographic data (NSTDB 1:10 000) were provided through the Geographic Information Science Centre at Dalhousie University and are property of Service Nova Scotia and Municipal Relations. The wind data were obtained from the Historical Climate Data on the Environment and Climate Change Canada website.

2.3 Approach/Photos/Time Periods

The time periods assessed were based on the availablity of aerial photographs of the Minas Basin coastline. For data management, the Minas Basin system was divided into six smaller sections (Figure 2.1) and was analyzed by section before the data were compiled to derive erosion rates and volumetric sediment input for the entire system.

Two time periods were examined in this thesis based on the availability of aerial photographs. These periods are stated throughout the thesis as 1964 - early 1990's and early 1990's - 2013. Different sections of coastline were photographed in different years, which helped to determine the sections for assessment as well as the two time periods. Years used for each section are shown in Table 2.2. Satellite imagery available in ArcMap from 2013 was used to identify the modern coastline. Photos taken at both high and low tide could be used since erosion of mudflats or salt marshes were not taken into account. Evaluation of coastal erosion was completed using these images with GIS.

Figure 2.1: Sections 1-6 for Minas Basin erosion analysis. Blue dots show field site locations where cliff height measurements were taken.

Table 2.2: Dates of aerial photographs and satellite imagery used for each section

Section	Aerial Photos	Satellite Imagery
1	1964, 1995	2013
2	1964. 1994	2013
3	1964, 1994	2013
4	1964, 1992	2013
5	1964, 1992	2013
6	1977, 1992	2013

2.4 Erosion Measurement

2.4.1 Coastline Creation

Photographs were georeferenced to the base satellite imagery with the *georeferencing* toolbar in ArcMap using control points at road intersections and buildings. The base imagery was projected using the UTM zone 20 coordinate system from the NAD83 datum to minimize distortion. Numerous control points, evenly distributed, were used to ensure accuracy. Finding suitable control points was challenging for some photos as often half the photo was of mudflats or water. The coastline also cannot be used as a reference since it is constantly changing. Distortion can occur along the edges of photographs. To minimize this, photos that overlapped were chosen and added to a mosaic dataset. The edges of the photos were erased using the *build footprints* option so that they were not used in analysis.

The coastline was digitized for the three photo dates mentioned in Section 2.3. This was done by adding a new polyline shapefile in the ArcMap document, which was set to the same spatial reference. A new feature was created and the coastline was traced using the *pencil* tool in the *editing* toolbar for each photo.

Points were placed close together to ensure a good fit. To ensure changes between time periods were measured accurately, the coastine was always traced along the top edge of cliffs and the top edge of bluffs or dykes where cliffs are not present. Each year in each section (Figure 2.1) was completed separately.

2.4.2 Distance Measurement

The *Euclidean Distance* tool in the *Spatial Analyst* toolbar was used to create a distance file from the digitized coastlines. This tool measures orthogonal distance continuously along a line out to a set distance (100 m). This tool was used on the 1964 coastlines as well as the early 1990's coastline. Figure 2.2 shows an example of the output from a 1964 coastline. These distance files were then used when measuring the distance from the 1964 coastline to the early 1990's coastline and to the 2013 coastline, as well as from the early 1990's coastline to the 2013 coastline. Erosion rates could then be measured for each time

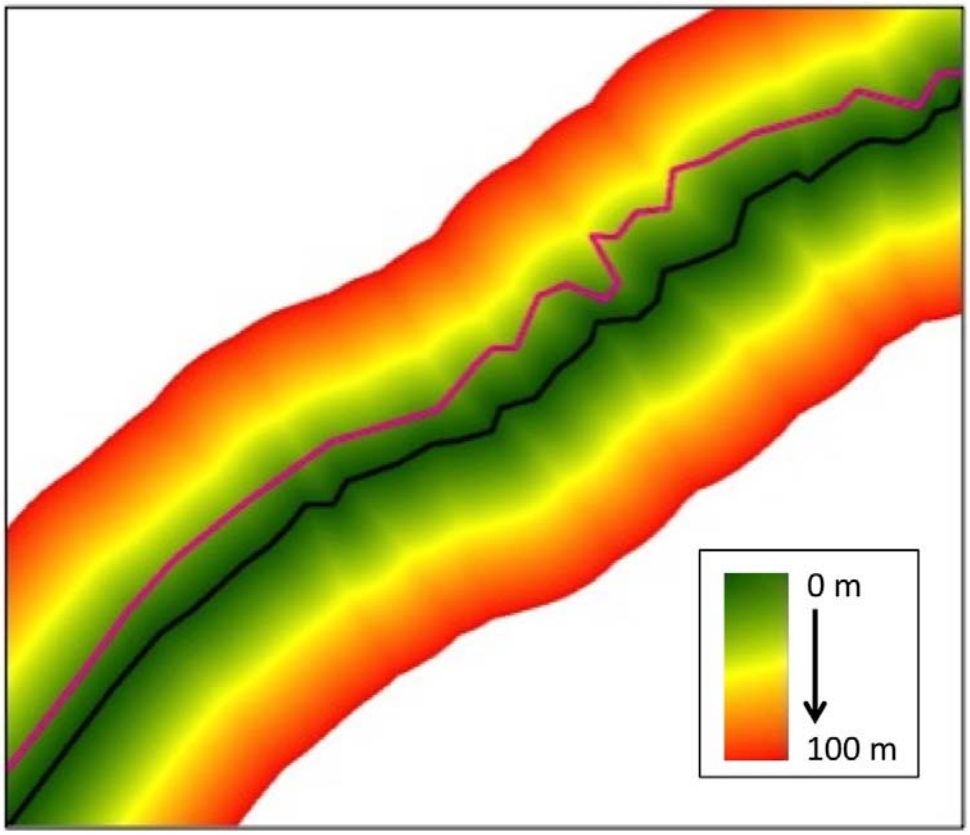

Figure 2.2: Example of *Euclidean Distance* tool output from a 1964 coastline. 2013 coastline in pink, 1964 coastline in black. Colours show distance from the 1964 coastline.

period as well as the overall study period. The process was the same for each section, so section 1 is used below as an example to describe the methods.

The 2013 and 1995 coastlines were interpolated using the distance files created above. The *interpolate shape* tool in the *3D Analyst* toolbox was used. The input feature was the coastline of the most recent time period and the input surface was the distance file from the oldest coastline. For example, if the erosion distance from 1995 to 2013 was to be measured, the 2013 coastline and the 1995 distance file would be used. The output file was a line with distance eroded values which was used in the *3D Analyst* toolbox to create a profile graph of the distance eroded along the line for each section. These data were exported in a table for further analysis. For analysis purposes discussed later, the polyline outputs from this step were split into 500 m sections using the *split line* option in the *editor* toolbar.

To compare erosion values between sections, erosion rate (m/yr) was calculated. This was completed in the attribute table by adding a field and using the *field calculator* to divide the total erosion amount for each section along the line by the number of years over which the erosion occurred.

Analysis of variance (ANOVA) was completed to test for significant difference in erosion rates between the 6 sections using overall rates (1964 - 2013). A paired-t test was used to look for significant changes in erosion rates between time periods for the entire coastline as well as within each section. A 95 % confidence interval was used for all statistical tests.

2.4.3 Area Measurement

In order to quantify the total area of land lost to coastal erosion, polygons had to be created using the digitized coastlines. This was completed by connecting two coastlines in an editing session at the end of each section and merging the coastlines using the *merge* tool to create a single shapefile. The connected polyline was converted to a polygon using the *feature to polygon* tool (Figure 2.3). To get the area eroded from 1964 to 2013 the 1964 and 2013 coastlines were merged and converted. The area of the polygon was then calculated by creating a new field in the attribute table and using the calculate geometry

option in the *field calculator*. The sum of this field could then be calculated to get the total area eroded for that section.

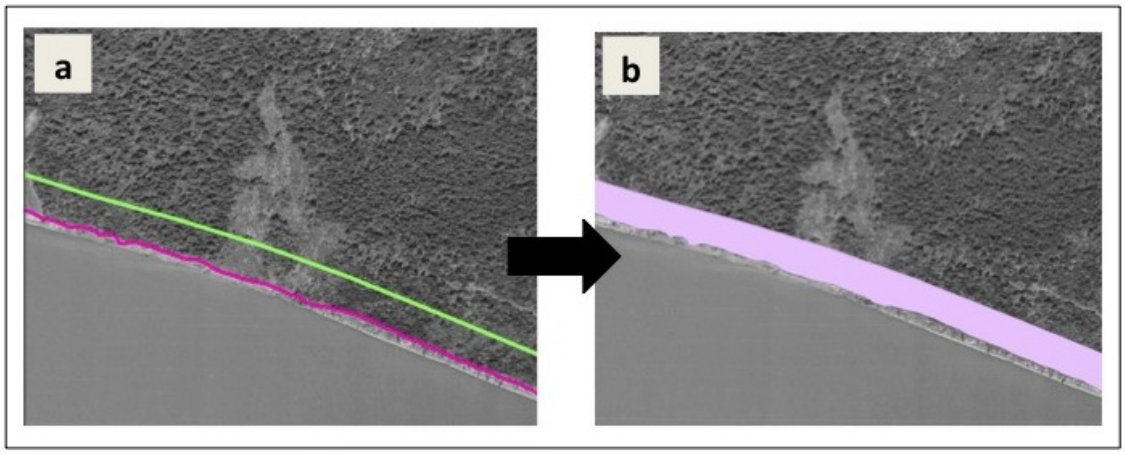

Figure 2.3: Example of area polygon creation. a) 1964 coastline (pink) and 2013 coastline (green) over a 1964 aerial photograph. b) Area of coastline eroded from 1964 to 2013.

2.5 DEM Creation

A digital elevation model (DEM) was created in order to be able to calculate the volume of sediment being eroded. Ideally, a DEM created from LiDAR data would be used as it is the most detailed and accurate. There are LiDAR data for most of the Minas Basin area, but they were not available for this study. Therefore, a DEM was created from the NSTDB 1:10 000 topographic county maps available through the GIS Centre at Dalhousie.

The elevation contours for Kings, Hants, Cumberland and Colchester counties were merged and then clipped to the study area. The *Topo to Raster* tool was then used to create a DEM (Figure 2.4). The original topographic data have a resolution of 5 metres. The DEM created has a pixel size of 1 m.

A sample DEM created from LiDAR data was provided by Dr. Tim Webster from the Applied Geomatics Research Group at COGS (Center of Geographic Sciences). This DEM covered two small sections where field measurements had been taken, so they could be compared with both field data and topgraphic maps.

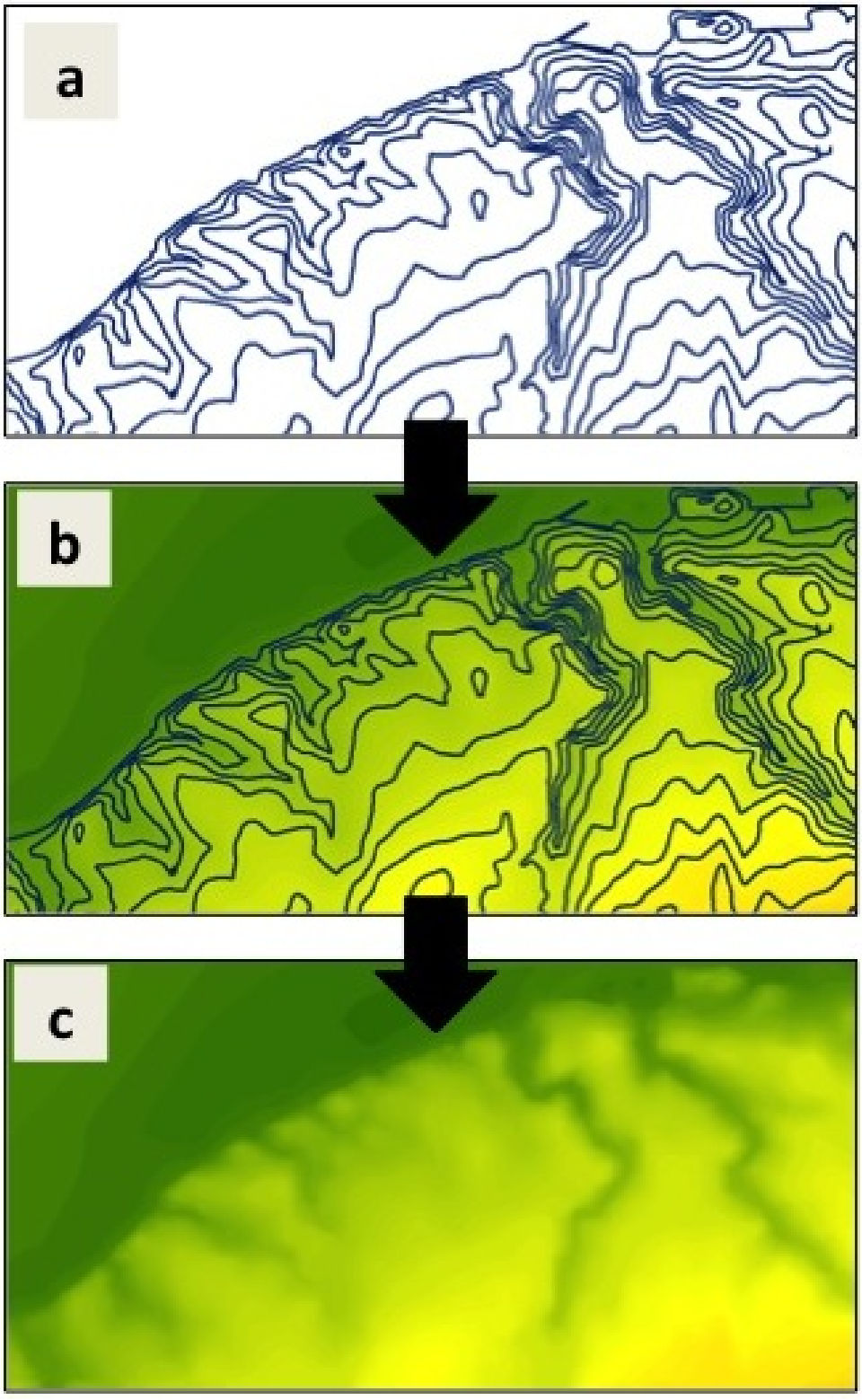

Figure 2.4: Example of creating a DEM from topographic contours. a) original topographic contour map with 5 m resolution. b) Contours over created raster DEM c) Created DEM with 1 m resolution.

2.6 Field Data

Cliff height measurements were taken at 64 sites around the Minas Basin (Figure 2.1) to compare elevations from a Theodolite application (Hunter Research and Technology, LLC) to those from the created DEM as well as the sample LiDAR DEM. Sediment samples from the cliff and beach were taken at each field site (*Ruhl*, 2016).

2.6.1 Angle Measurements

The Theodolite application measures the angle between two points. The angle from the top of the cliff to a point 15 m out from the cliff base (ridge angle) was measured as well as the slope of the beach (horizon angle), and the slope of the cliff face itself (cliff angle) (Figure 2.6). It also takes a photograph with the location coordinates as well as the angle recorded for each measurement (Figure 2.5).

Figure 2.5: Example photographs taken with the theodolite application. Top photo shows elevation angle to top of cliff taken from 15 m out from the cliff base. Bottom photo shows the slope angle of the cliff face being measured.

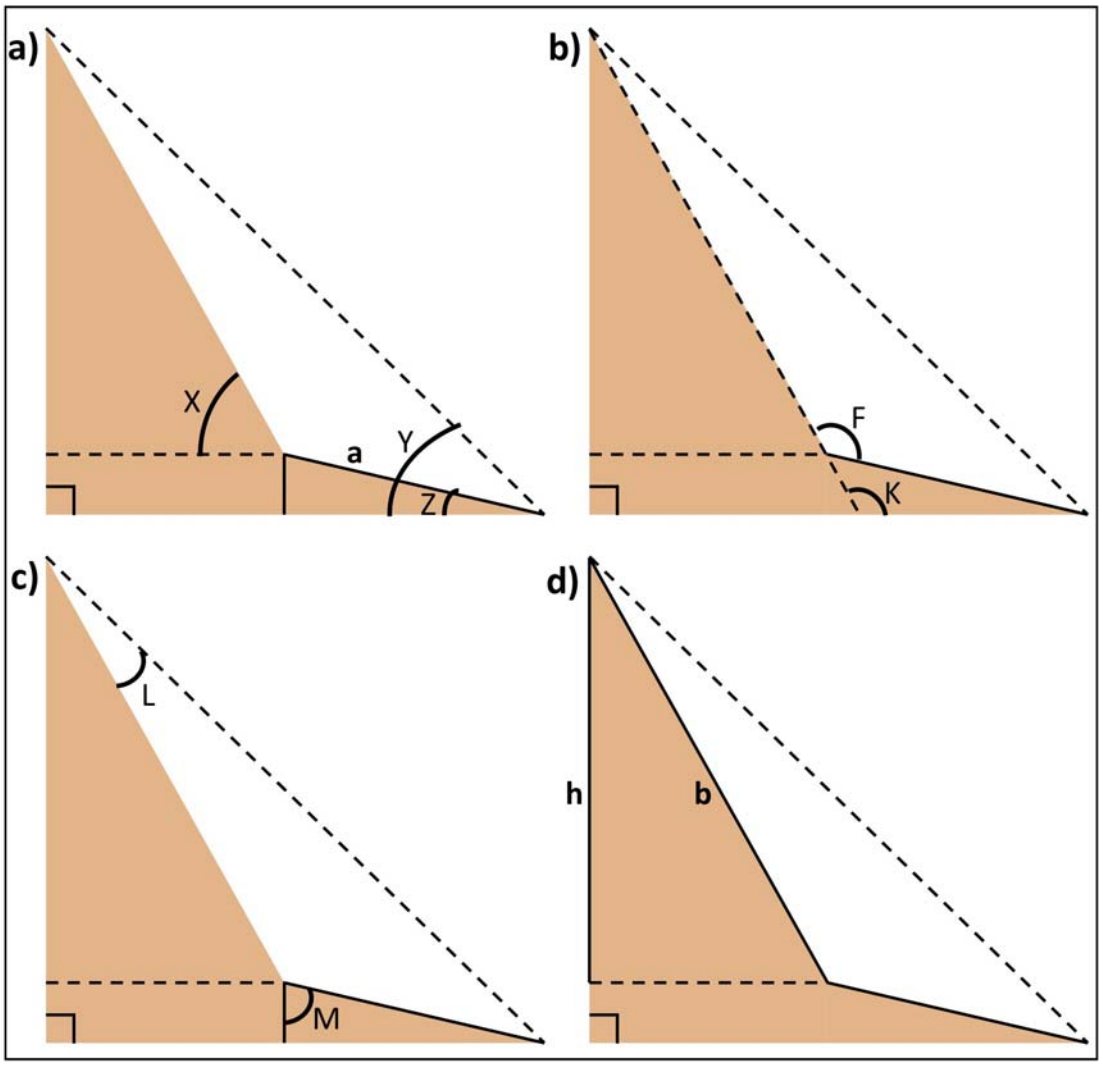

Figure 2.6: **a)** *Measurements taken in the field.* X is the cliff angle, Z is the horizon angle, Y is the ridge angle and a is the distance from the cliff base to the location the measurements were taken. **b)** *Angle calculations.* K and M found using supplementary angles **c)** *Angle calculations.* M and L found using sum of interior angles **d)** *Calculating height of cliff.* b and h found using law of sines.

2.6.2 Height Calculations

The angles measured at the field sites with the theodolite application (Figure 2.6) were then used to calculate cliff heights at each site. These calculations were completed using basic trigonometry. The details of these calculations are outlined in Appendix A.

Two sites had stair access up the cliff faces, where extra measurements of the height were taken and compared to the calculated measurements. The Lower Economy site has

a wall that was erected in 1987. The distance the cliff has eroded behind this wall was measured and an erosion rate calculated. This rate was then compared with the 1994 to 2013 erosion rate calculated from the aerial photographs.

2.7 Volume Calculations

To get measurements of the total volume of sediment eroded, the area polygons were multiplied by the elevation data. The first step was to convert the vector polygons to raster files using the *convert to raster* tool (Figure 2.7b). The cell size of the rasters created matched those of the DEM (1,1). The *extract by mask* tool was used to to extract the DEM for the shape of each polygon or eroded area (Figure 2.7d). The input raster is the DEM and the input feature is the polygon rasters.

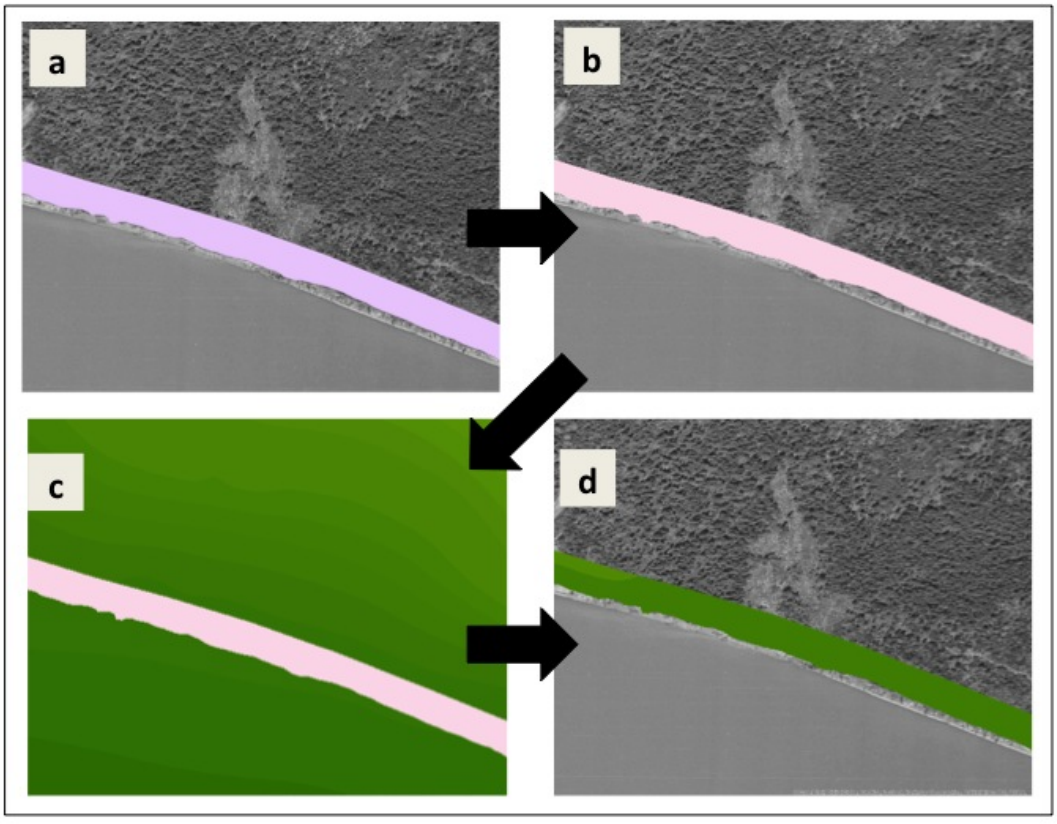

Figure 2.7: Example of methods to calculate volume eroded. a) Initial vector polygon of area eroded. b) Raster polygon of area eroded with a 1 m cell size. c) Raster polygon over DEM. d) DEM clipped to raster polygon.

Volume of sediment for each polygon was calculated using the *surface volume* tool in the *3D analyst* toolbox. This tool allows for the volume to be calculated for each of the DEM polygons above the beach elevation value in each polygon which helps to account for the fact that the bottom of the area that is being eroded is not always at sea level. Total volume results were exported as text files. An assumption was made that the base of what is being eroded is flat where in some cases it would most likely be on a slope. This would lead to a slight overestimation in the volume measurements.

Volume input rates were determined for both time periods in each section, as well as overall. The same statistical tests were carried out for these values as were completed for erosion rates.

2.8 Mass Calculations

To find an estimate of the mass of sediment eroded and entering the Minas Basin system from coastal erosion sources, the calculated volumes were multiplied by the density of the rock in the cliffs. Not all of the coastline eroded is comprised of Triassic sandstone cliffs, but the amount of sediment from cliff sources dominates any input from smaller bluff, drumlins and marsh/dyke erosion. Cliff characteristics were deemed sufficient to roughly estimate mass input. The density value that was used was the density of quartz (2.65 g/cm^3). The density of quartz was chosen because 79% of the of the Minas Basin coastline is composed of Triassic Sandstone (*Amos and Long*, 1980) and quartz is the primary mineral.

The porosity of the material being eroded also was considered. The porosity of the Wolfville formation, which makes up most of the Minas Basin coastline, is 1-17% for surface sections (*Kettanah et al.*, 2013). A calculation (Equation 2.1) was completed for the minimum, maximum and mean porosity values.

$$mass = density \times volume \times (1 - porosity) \tag{2.1}$$

2.9 Erosion Analysis

Statistical analysis was conducted to determine if any local factors showed significant correlation to areas of increased erosion. First, a wind fetch model was created and then physical properties available in the NSTDB 1:10 000 topographic county maps were compared to the erosion rate data. The erosion rate data that were used for the following analysis was the rate averaged over the entire study period.

2.9.1 Wind Fetch Model

A GIS model from the UMESC (Upper Midwest Environmental Sciences Centre) based on scripts written by David Finlayson (*Rohweder et al.*, 2012) was used to calculate wind fetches for the Minas Basin. First, a raster map of the Minas Basin with 100 m by 100 m resolution was created from the NSTDB map using the *polygon to raster* tool. The map was converted to a binary map with 1 representing land and 0 representing water.

Wind data were obtained from Environment Canada historical climate database. The Truro/Debert station was used as it contained the most complete and continuous wind data over the study period. Daily wind direction data were compiled and sorted to find the percent of time the wind came from each direction, by degrees 0 to 350. These data were saved in a text file to be imported into ArcMap.

The *Wave Model* tool in the *Waves (2012)* toolbox (*Rohweder et al.*, 2012) was used to create the wind fetch model of the Minas Basin. The land raster map and the wind direction text file were put into the tool and the *calculate weighted fetch* option was selected. This allowed the fetch to be calculated individually for each direction as well as for an overall map of fetch to be created based on the percent of time the wind blows from each direction in the system. The wind fetch map produced was used in the spatial statistics analysis to assess any correlation between wind fetch and erosion rates.

2.9.2 Spatial Statistics

Several physical features of the Minas Basin system were assessed as possible causes of increased erosion rates. The factors assessed were bedrock formation geology, surficial

geology, terrain, soil drainage, soil texture, forest cover, elevation, windfetch and salt marsh location. Data were obtained from the NSTDB 1:10 000 topographic maps.

The erosion polyline for the entire study period was used for this analysis. The line from each section was merged, so the analysis was completed for the entire Minas Basin coastline together.

Each factor was added to the erosion polyline using the *spatial join* tool with a one to one join. The join feature was each factor and the target feature was the erosion polyline. The search radius was set to 100 m. An ANOVA was completed to test for relationships between variables in each factor and erosion rates. Linear regression was used to test for corrleation of erosion rates with wind fetch and elevation as these are continuous data sets not categorical.

CHAPTER 3

RESULTS

3.1 Erosion Rates

Over the entire study period, erosion rates along the coast of the Minas Basin varied from 0 m/yr to 1.4 m/yr (Figure 3.1). The highest erosion rates are found between Five Islands and Parrsboro, the north western shore of Cobequid Bay, to the west of Walton, and near Selma and Blomindon. Overall erosion rates are highest in section 1 with an average of 0.5 m/yr. Section 3 and 6 showed the lowest erosion rates with an average of 0.34 m/yr and 0.35 m/yr (Figure 3.3). Section 1 has erosion rates significantly higher ($p < 0.05$) than sections 3, 4, 5 and 6. Erosion rates in section 2 are significantly higher than sections 3 and 6 (Figure B.1). The mean erosion rate is 0.42 m/yr for the entire coastline.

Erosion rates have increased significantly over the two time periods assessed ($p = 0.001$) (Figure 3.2). Time period one shows a mean erosion rate of 0.39 m/yr (S.D. = 0.25 m/yr), where time period two shows a mean erosion rate of 0.48 m/yr (S.D. = 0.30 m/yr). Erosion rates have significantly increased ($p < 0.05$) in sections 1-5, with section 5 showing a smaller increase. There was a significant decrease ($p < 0.001$) from 0.46 m/yr in time period one to 0.27 m/yr in time period two in section 6 (Figure 3.3). The most notable increase occured between Five Islands and Parrsboro, along most of the Cobequid Bay coastline, and near Walton (Figure 3.4). The greatest increase in erosion rate occured in section 3 where the mean rate rose from 0.23 m/yr to 0.49 m/yr (Figure 3.3).

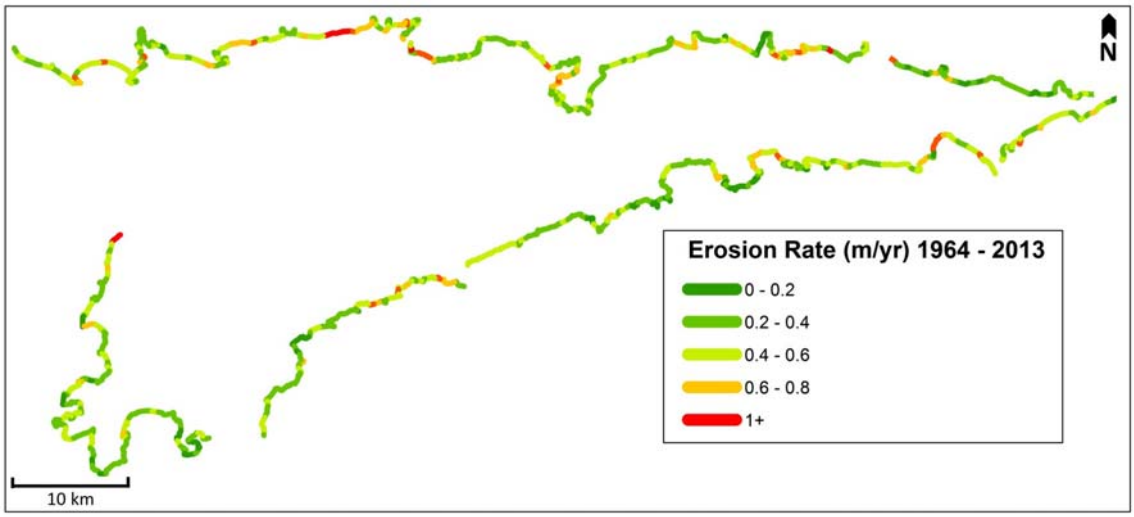

Figure 3.1: Rates of coastline erosion around the Minas Basin based on aerial photographs from 1964 to 2013. Rates are averaged over 500 m sections.

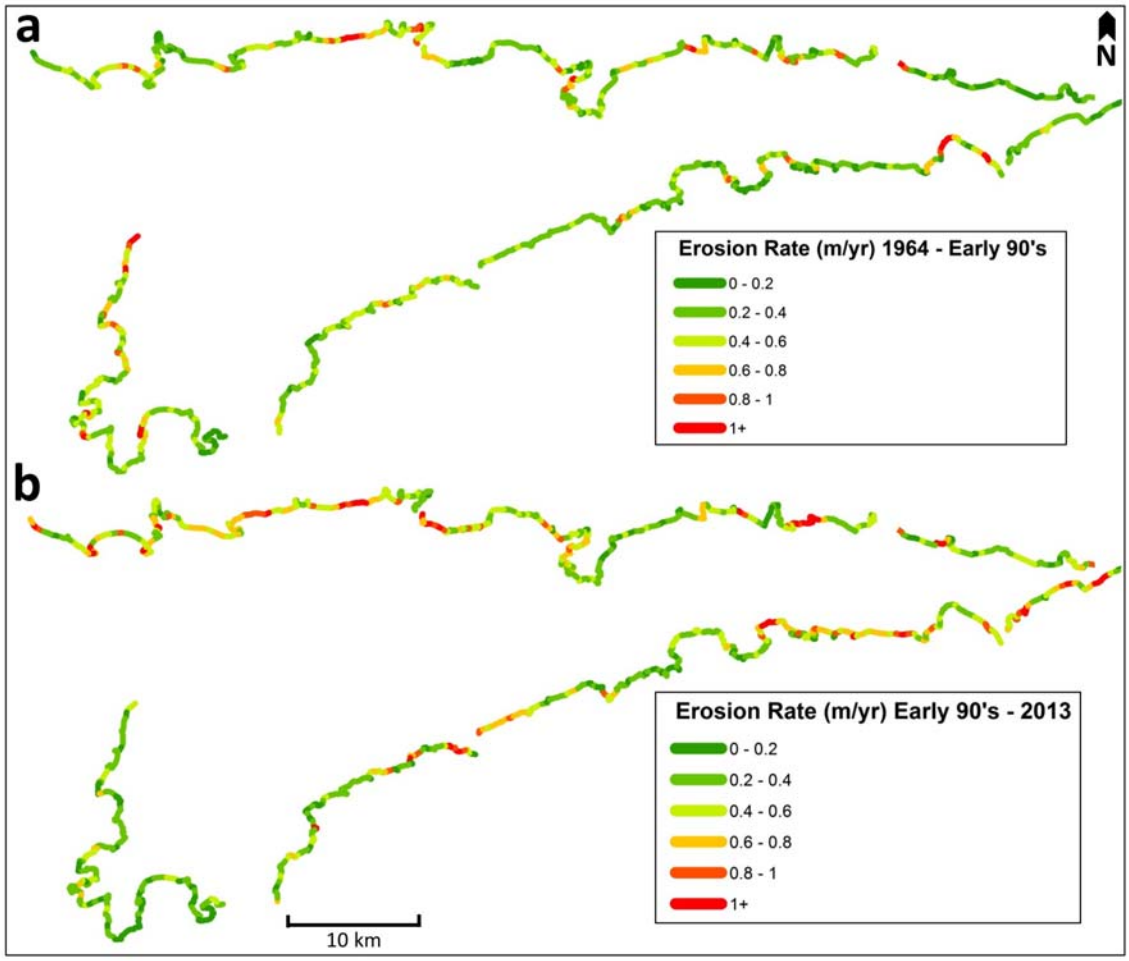

Figure 3.2: Rates of coastal erosion around the Minas Basin over two time periods from a) 1964 to the early 1990's and b) from the early 1990's to 2013. Rates were measured from aerial photographs and were averaged over 500 m sections.

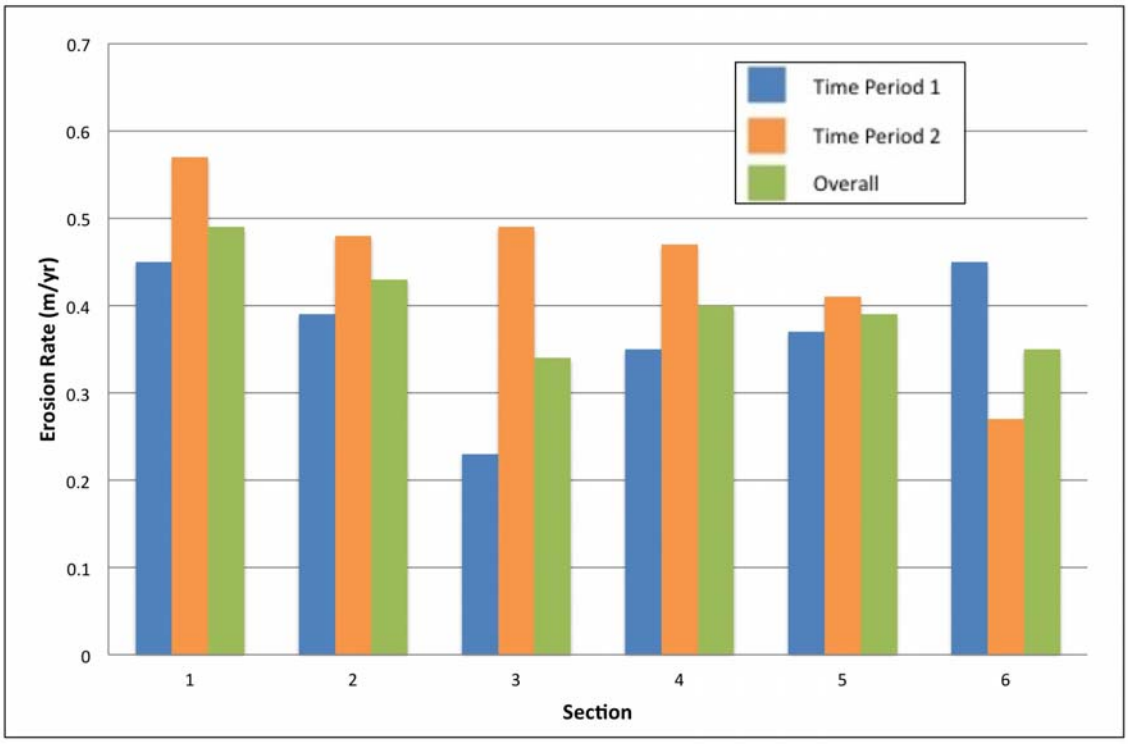

Figure 3.3: Coastal erosion rates by section for time period 1 (1964 to early 1990's), time period 2 (early 1990's to 2013) and overal (1964 to 2013).

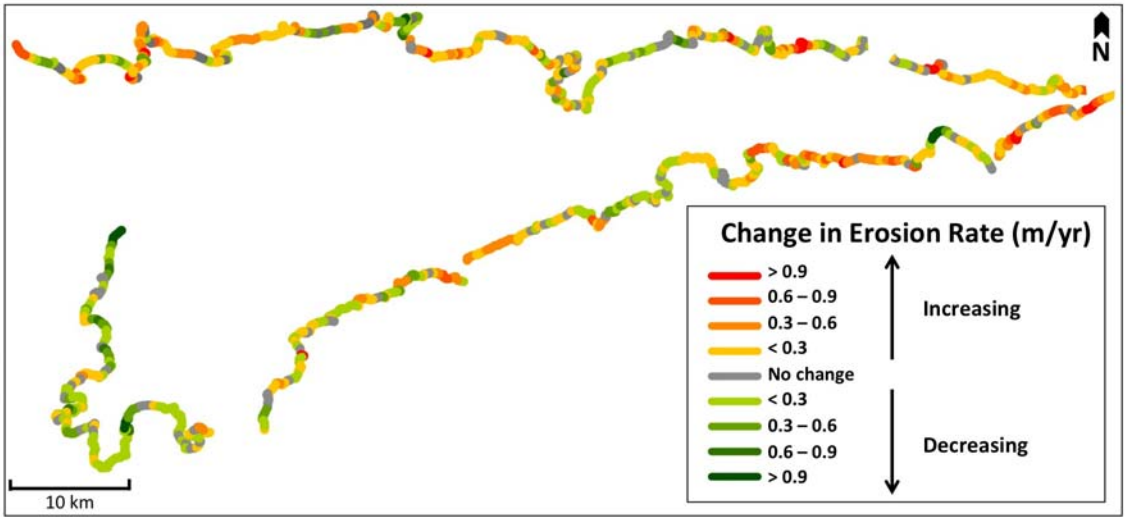

Figure 3.4: Illustration of the changes in linear erosion rates along the coast of the Minas Basin between the two time periods assessed.

3.2 Lower Economy Site Comparisons

The Lower Economy field site provided a location to test the accuracy of the GIS methods for measuring cliff erosion. This location has a wall made of large wooden posts that were placed in the beach at the base of the cliff in 1987. The cliff has since eroded behind this wall and the distance was measured directly (4.2 m) giving an erosion rate of 0.15 m/yr. From the aerial photographs this site had an erosion rate of 0.26 m/yr from 1994 - 2013. Direct field measurements were taken at the base of the cliff and measurements from the photos were taken from the top of the cliff, so this could account for some of the error if the cliff was not eroding evenly. Also, the time periods over which they were measured are different, this could explain the discrepency in the erosion rates.

Figure 3.5: Erosion behind wall constructed against cliff base in 1987 in Lower Economy, Nova Scotia.

3.3 Cliff Height Measurements

Elevation values from the topographic map created from the elevation contours of the NSTDB maps (Topo) were compared to elevations from the same location from a sample Digital Elevation Model constructed from LiDAR data. The values were compared (Figure 3.6) with the DEM values assumed to be the most accurate measure of elevation. The data show a significant linear regression ($p < 0.001$) and the slope of the regression line is 1.017 showing strong agreement between the DEM elevations and the elevations on the topographic map (RMS = 2.5).

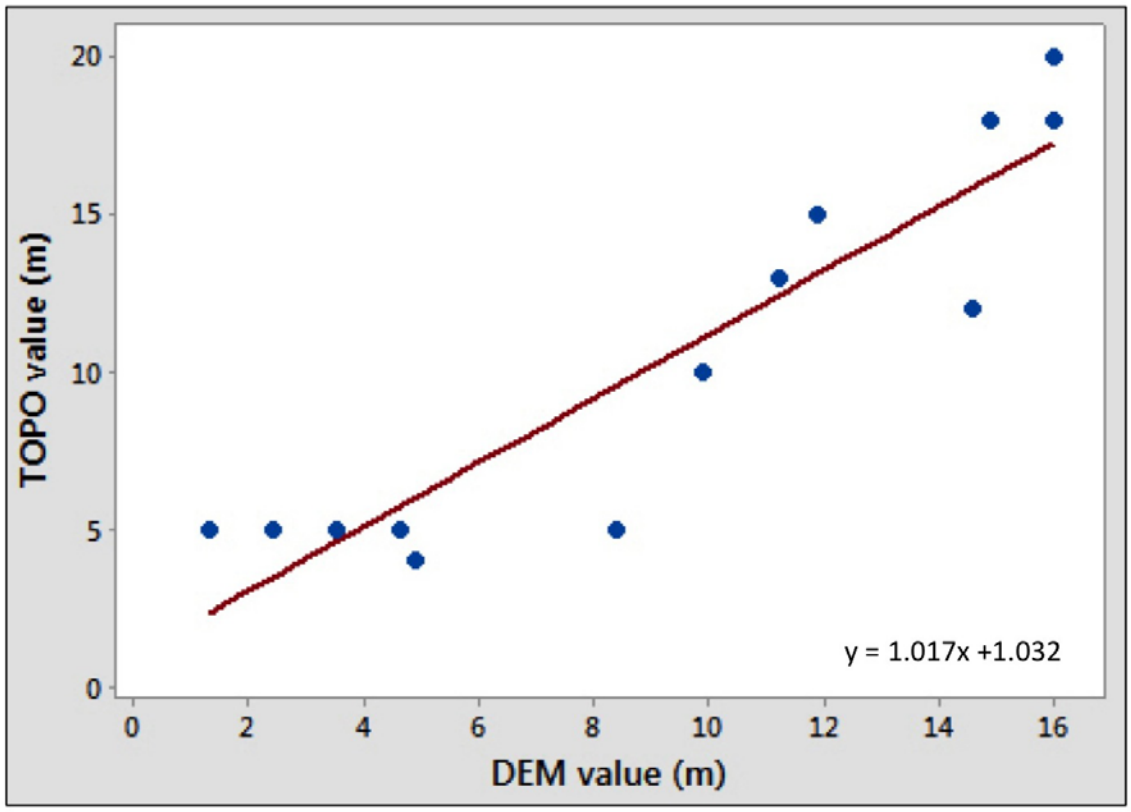

Figure 3.6: Elevations taken from DEM created from LiDAR data compared with elevations measured from elevation map created from topographic contour data. Data show a significant linear regression ($p < 0.001$).

Cliff height measurements taken in the field with the theodolite application were compared to the TOPO values (Figure 3.7) to test the accuracy of the theodolite app as a field method. Measurements showed a resonable fit, but the calcuated heights varied more from the TOPO values as the cliff heights increased (Figure 3.8a) (RMS = 5.8). While

calculated and topographic heights show significant linear correlation ($p < 0.001$), with the removal of cliff heights over 25 m, the slope of the regression line falls much closer to the 1:1 line (RMS = 2.4)(Figure 3.8).

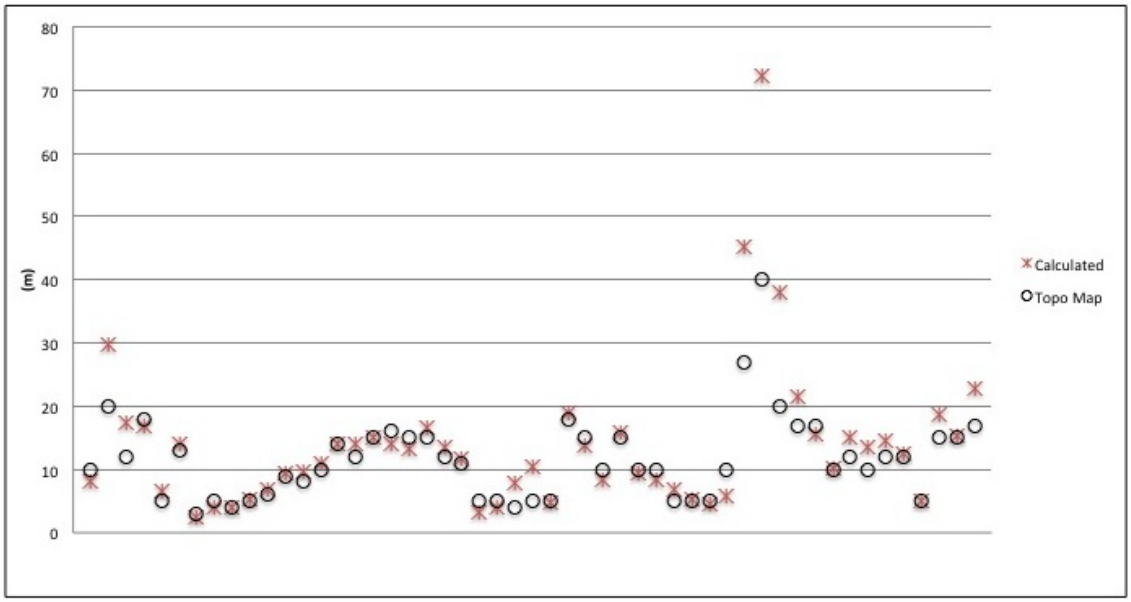

Figure 3.7: Elevations from elevation map created from topographic contour data compared with field cliff height calculations using angles measured with the theodolite app.

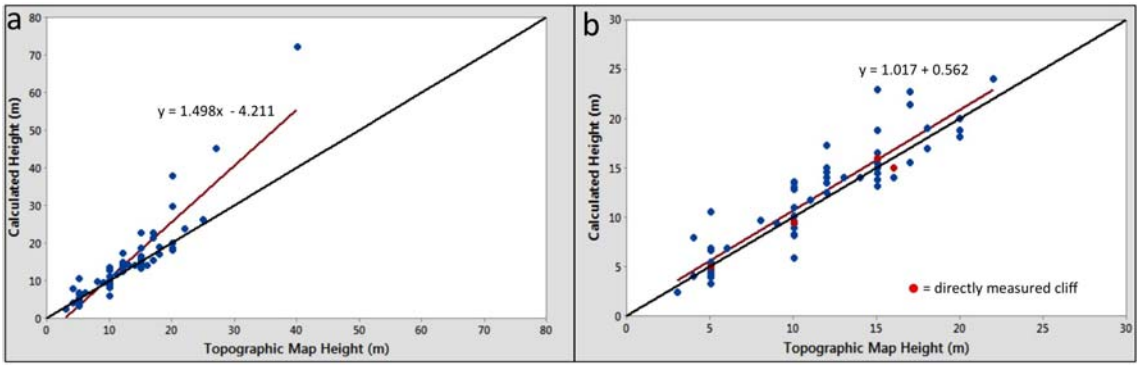

Figure 3.8: Elevations from elevation map created from topographic contour data compared with field cliff height calculations using angles measured with the theodolite app. Linear regression lines shown in red. 1:1 line shown in black. a) All of the data points measures in the field. b) Measurements with elevations over 25 m removed. Cliffs that were measured directly are shown in red.

The DEM that was created from the topographic contours was linked to the digitized coastline. Figure 3.9 displays the elevation of the coastline along the Minas Basin averaged over the 500 m sections used in the linear erosion and volumetric input maps. The highest

coastline elevations are seen along the nothern shore of the Central Basin.

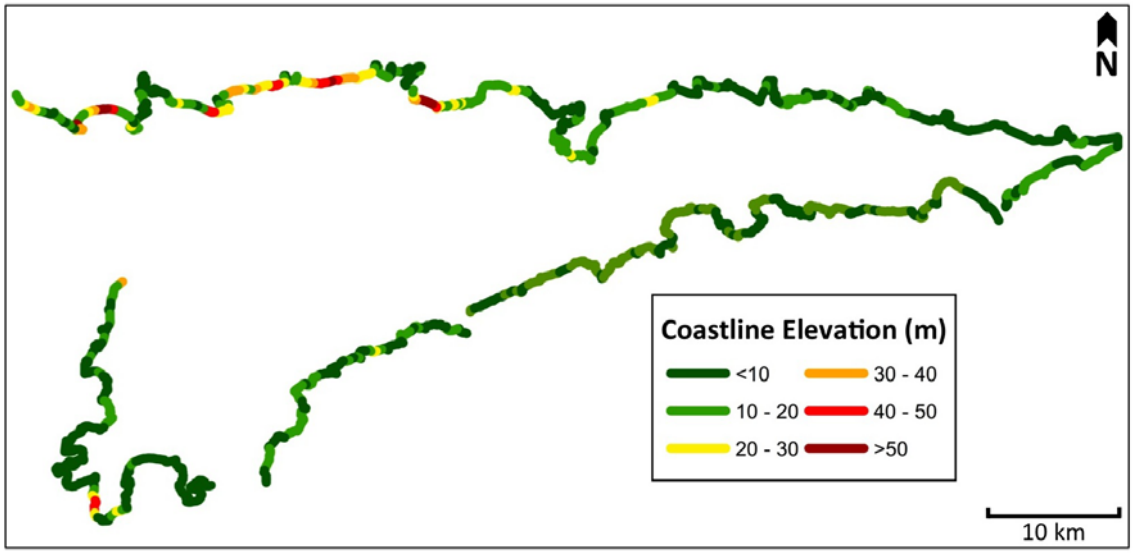

Figure 3.9: Coastline elevations along the Minas Basin coast from the topographic DEM. Averaged over 500 m sections.

3.4 Volume Input

Volume input rates over the entire study period along the coast of the Minas Basin range from 0 m^3/yr/m to 75.6 m^3/yr/m (Figure 3.10). The largest volume inputs are between Five Islands and Parrsboro and near Blomidon. This is the same area as some of the highest erosion rates, and also corresponds to areas of high coastline elevation. Overall volumetric inputs are significantly higher ($p < 0.001$) in section 1 than any other section (Figure B.2), with an average of 11.2 m^3/yr/m. Volumetric input rates are lowest in section 6 with a value of 3.4 m^3/yr/m, however this value is only signifiantly lower ($p < 0.001$) than input rates from section 1 and section 2 (Figure B.2). The mean volumetric input rate for the entire Minas coastline is 5.7 m^3/yr/m.

The volumetric input rates have increased significanly ($p < 0.001$) in sections 1-5 (Figure 3.11, 3.13). This is the same as what was observed with the erosion rates except for section 5, where there was no significant change in erosion rates. Section 6 observed a significant decrease ($p < 0.001$) in volumetric input from time period 1 to time period 2. For the overall basin, time period 1 had a mean input rate of 4.5 m^3/yr/m and time period 2 had a mean input rate of 6.3 m^3/yr/m. The largest increases were seen in section 1 and in section 3 (Figure 3.12), although the volume input from section 1 is nearly 4 times greater than the input from section 3. The increase in volumetric input in section 3 is assosicated with the increase in erosion rate. The increase in erosion rate in section 1 is not as large, but the cliff elevations are higher leading to a larger change in volumetric input. The total amount of sediment entering the Basin per year has increased from 9.0 x 10^5 m^3/yr in time period 1 to 1.3 x 10^6 m^3/yr in time period 2. This increase is not statistically significant ($p > 0.05$). This number, however, generalizes data over a large area, so it is more useful to look at the changes in individual sections to understand changes in volume input in the Minas Basin.

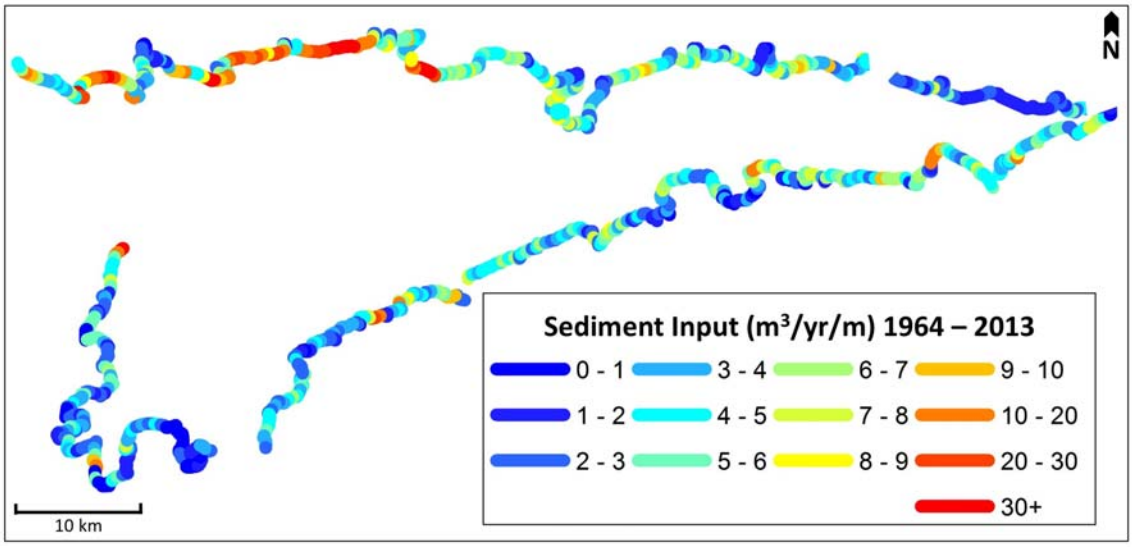

Figure 3.10: Rates of volumetric sediment input around the Minas Basin based on aerial photographs from 1964 to 2013 and elevation data. Rates are averaged over 500 m sections

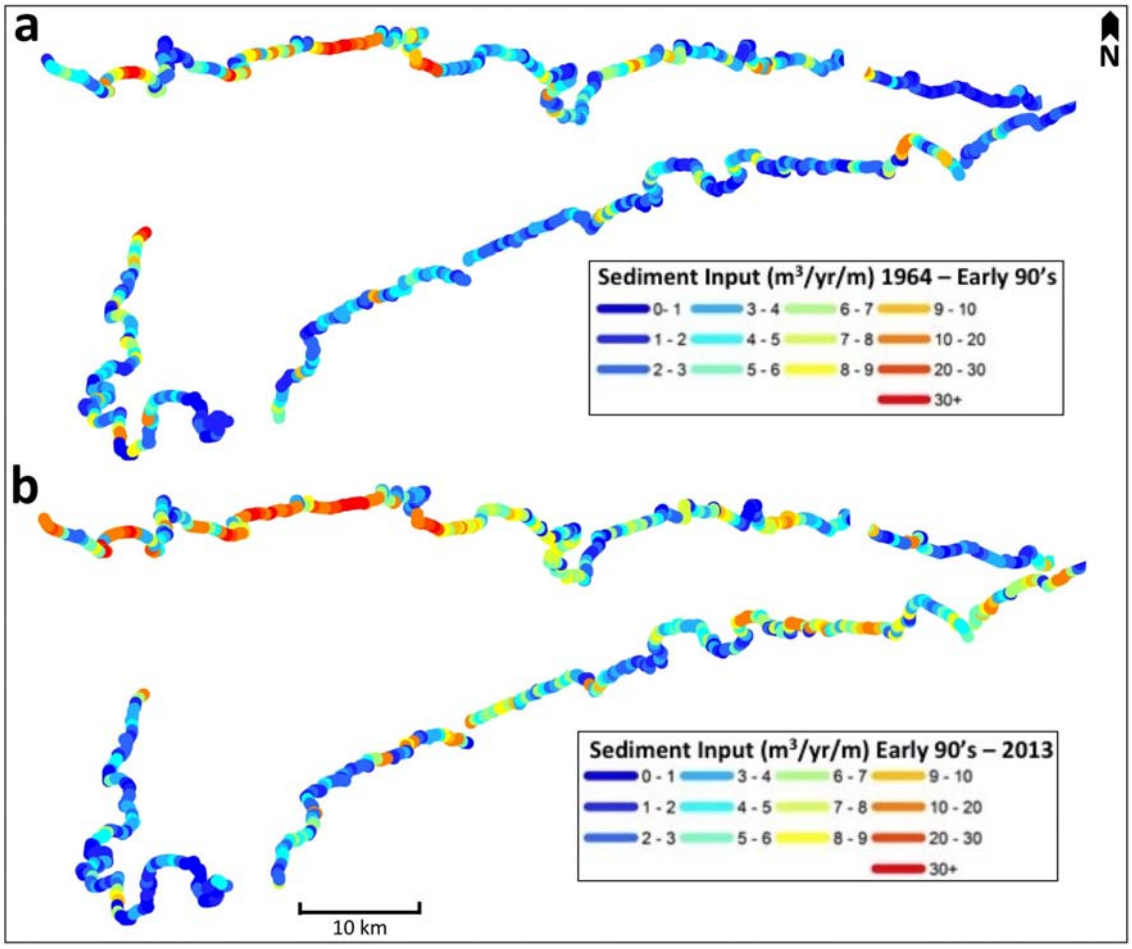

Figure 3.11: Rates of volumetric sediment input around the Minas Basin from a) 1964 to the early 1990's and b) from the early 1990's to 2013. Rates were measured from aerial photographs combined with elevation data and were averaged over 500 m sections.

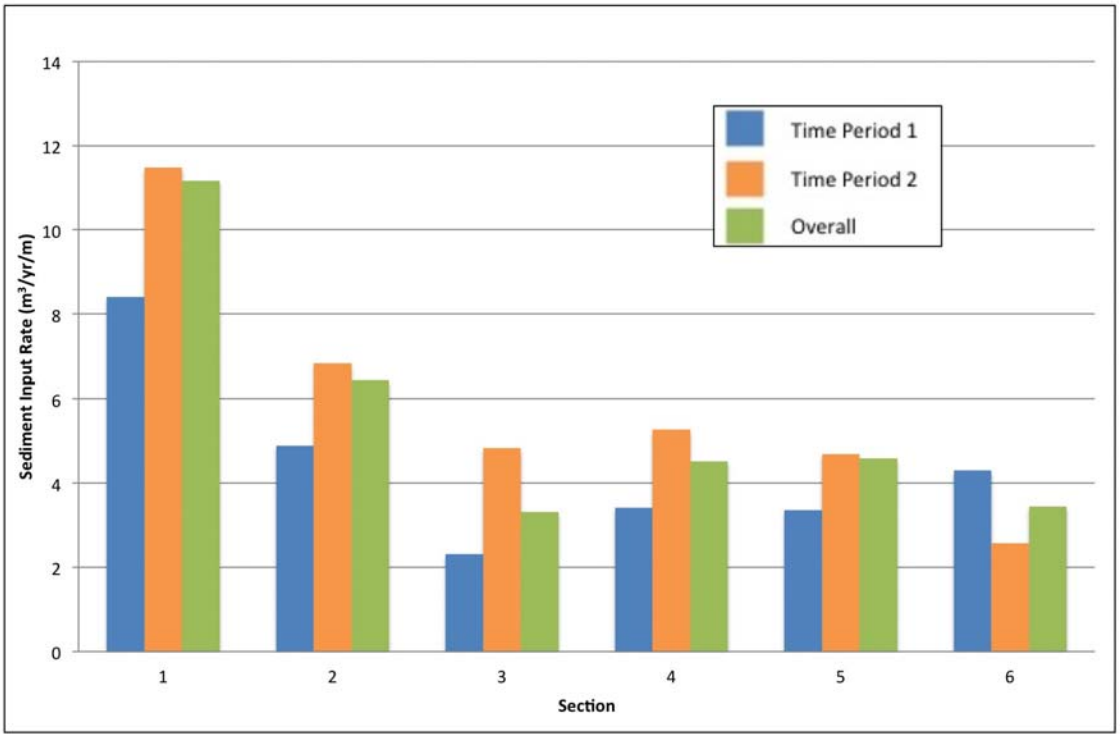

Figure 3.12: Rates of sediment input (m^3/yr/m) for both time periods and an overall average in for each of the 6 sections. Time period 1: 1964 - early 1990's, Time period 2: early 1990's - 2013

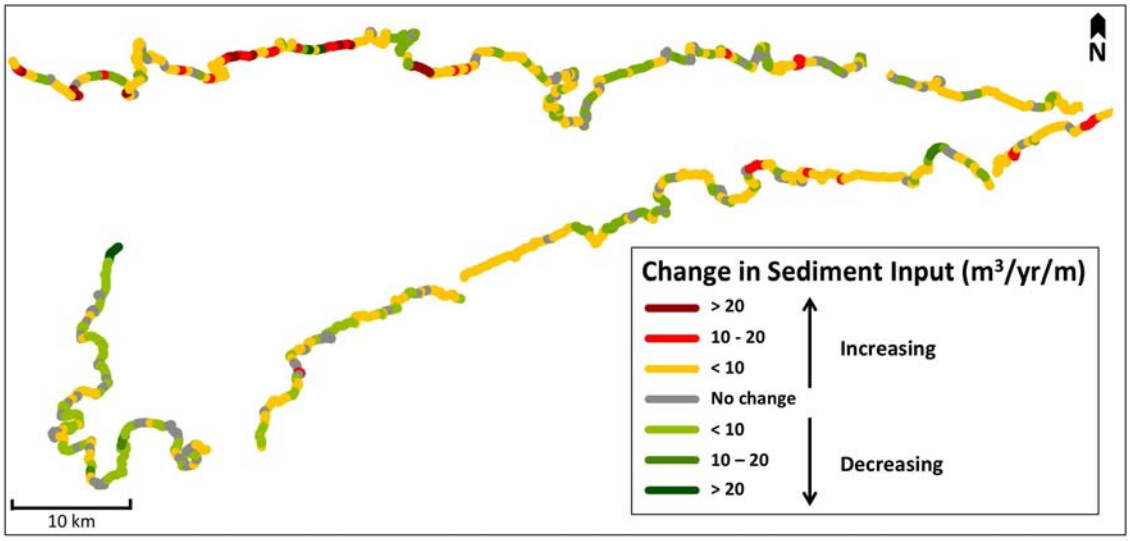

Figure 3.13: Illustration of the changes in sediment input rates along the Minas Basin coastline between the two time periods assessed.

3.5 Mass Input

An estimate of mass of sediment entering the Minas Basin system per year was made. This calculation assumed that the sediment being eroded was Triassic sandstone belonging to the Wolfville group which makes up most of the coastline of the Minas Basin (*Amos and Long*, 1980). Mass estimates ranged from 2.8 to 2.3 megatons per year as porosity increased from 0% to 17% (Figure 3.14).

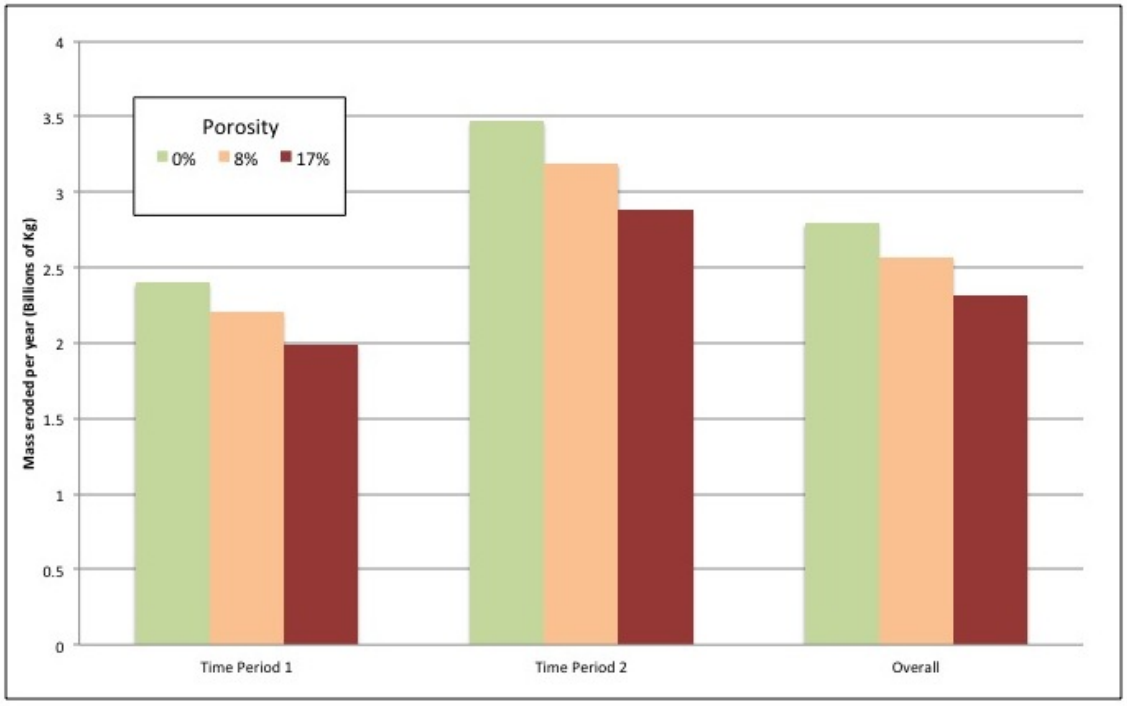

Figure 3.14: Mass of sediment entering the Minas Basin in each time period and overall for porosity values of 0, 8 and 17. Time period 1 is from 1964 to the early 1990's. Time period 2 is from the early 1990's to 2013.

3.6 Wind Fetch Model

Complied wind data from 1974 - 2013 near Truro shows the dominant wind direction to be from the west and slightly south west with the wind blowing from 250°, 260° and 270° at 8.3%, 10.6% and 9.9% of the time respectively (Table 3.15).

Wind fetch in the Minas basin ranges from near 0 up to 20 km. The wind fetch model output shows the largest wind fetch values to contact the coastline near Economy, Burntcoat Head and the northern shore of Cobequid Bay. The fetch is lowest along the coastline in section 6 as well as to the west of Economy Point and most of the southern shore of Cobequid Bay (Figure 3.16).

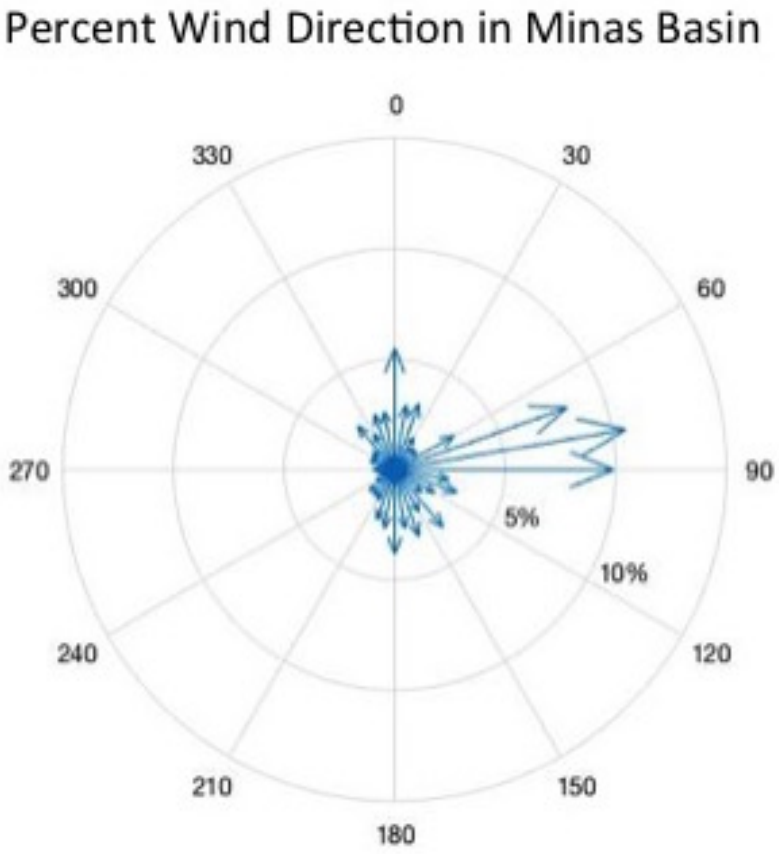

Figure 3.15: Wind rose showing the percent of time the prevailing wind blows in each direction. Data from Truro and Debert stations (Environment Canada historical climate database) from 1964 to 2013. Averaged daily direction of maxiumum wind.

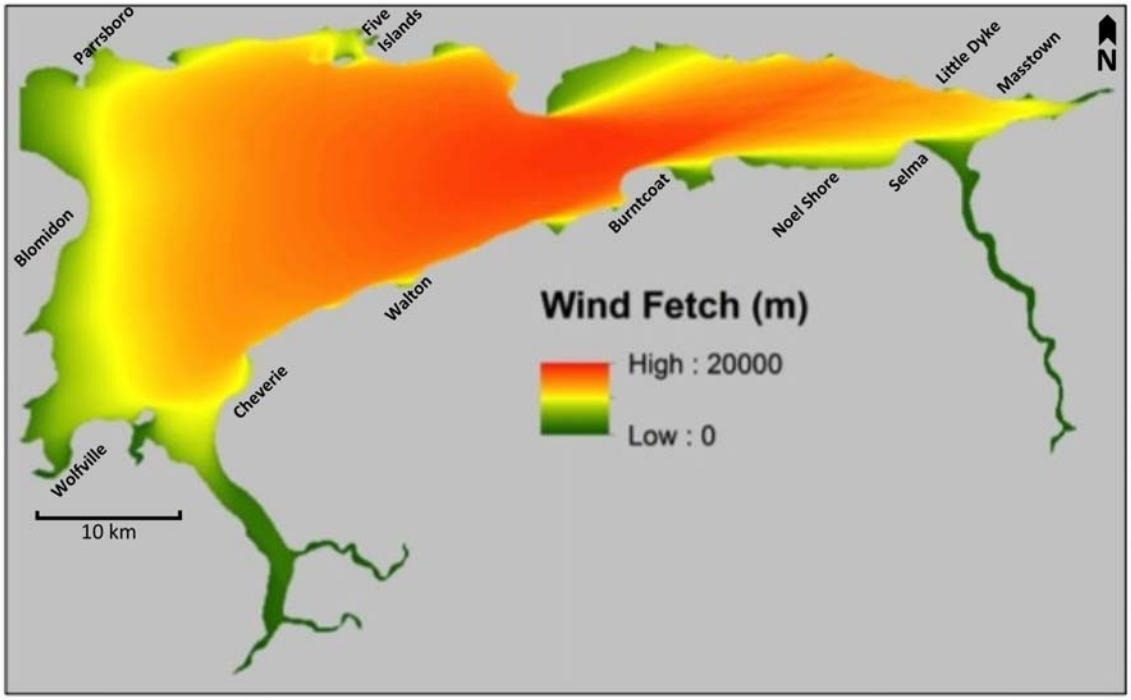

Figure 3.16: Wind Fetch model output based on wind direction percentages in Figure 3.15.

3.7 Salt Marsh and Dykes

Salt marsh locations plotted with the overall erosion rates for the Minas Basin show that in areas where salt marshes are located, lower erosion rates are observed (Figure 3.17a). Dykelines are shown in Figure 3.17b. Any erosion of dykelines contributes small amounts of sediment to the Basin compared to the much larger cliff sources. These areas are influenced by humans, because dykes undergo maintenance as they erode (*Asiedu*, 2013). Coastline sections indicated by 1 and 2 in figure 3.17b were omitted from the study. A dyke was built at 1 after the 1964 photos were taken, and one was built by 2 after the 1994 photos were taken.

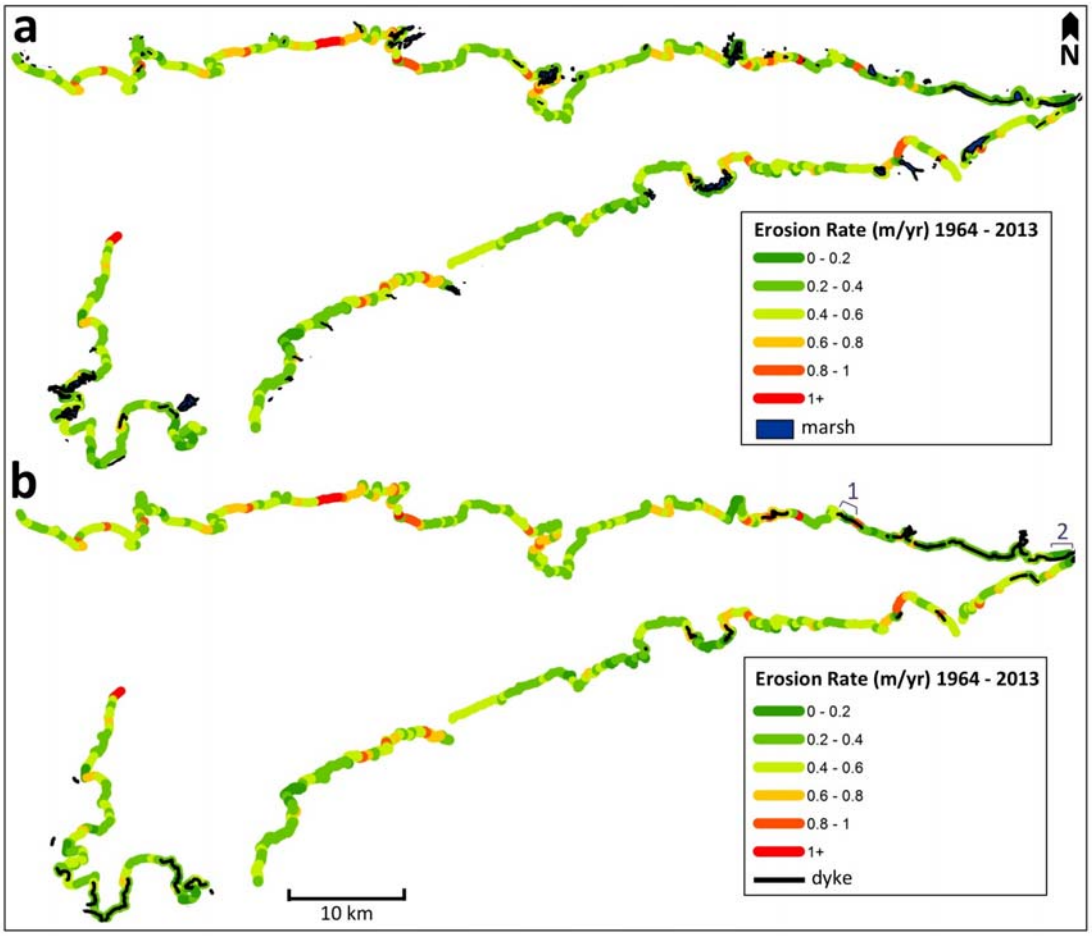

Figure 3.17: a) Salt marsh locations in the Minas Basin with coastal erosion rates (1964 - 2013). b) Locations of dykes along the Minas Basin coastline. Purple numbers 1 and 2 indicate locations where dykes were built during the study period.

3.8 Spatial Statistics

ANOVAs were completed to determine if any of the physical factors, such as bedrock geology, surficial geology, elevation, wind fetch, forest cover, soil texture and drainage, in the Minas Basin system could explain the variations in erosion rates observed along the coast. P values from the ANOVA output stated if the erosion rate associated with any variable within each factor was significantly different from that of at least one other variable. The 95 % confidence intervals could then be examined to see which variable showed the significant difference. Linear regression was completed for the wind fetch and elevation factors as these data are continuous not categorical. P values from the linear regression show if there is significant correlation between the factor and erosion rate. R values from the output can then show the strength of that correlation.

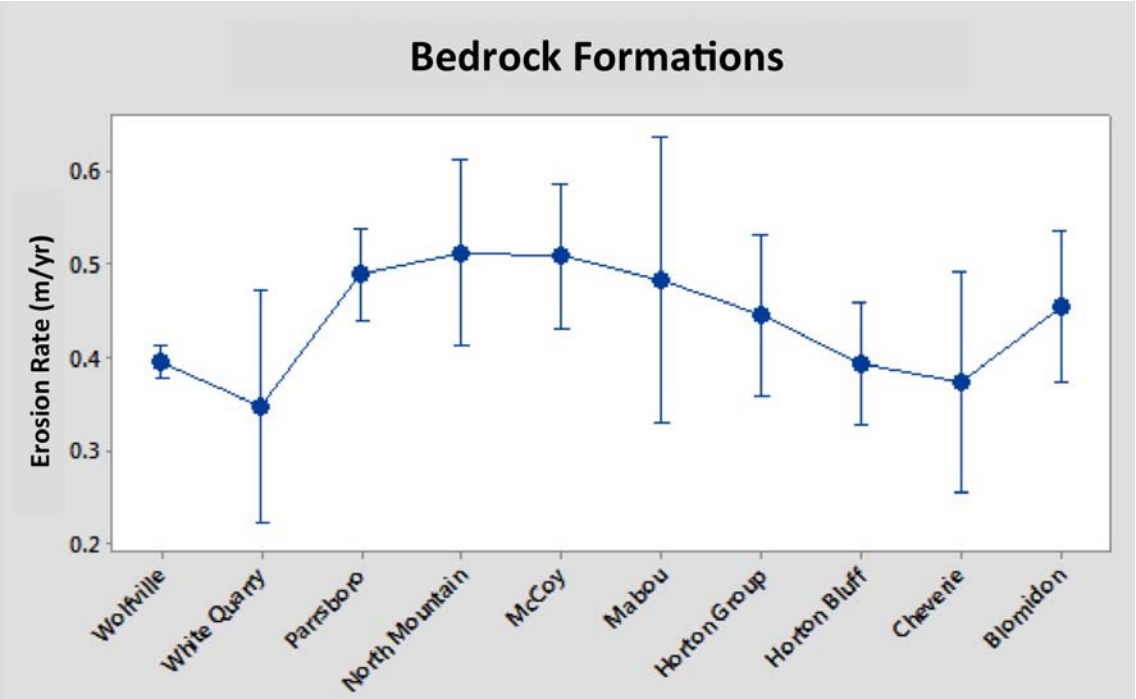

Figure 3.18: Erosion rate plotted against bedrock formations. 95 % confidence intervals are shown. p = 0.002.

The ANOVA for bedrock formation geology gave a p = 0.002. The Wolfville formation does show significantly lower erosion rates than the Parrsboro, North Mountain and McCoy formations (Figure 3.18). There is not one formation that shows significantly higher erosion rates than all of the other formations. Different types of surficial geology

show no correlation with erosion rates (p = 0.6) either (Figure 3.19).

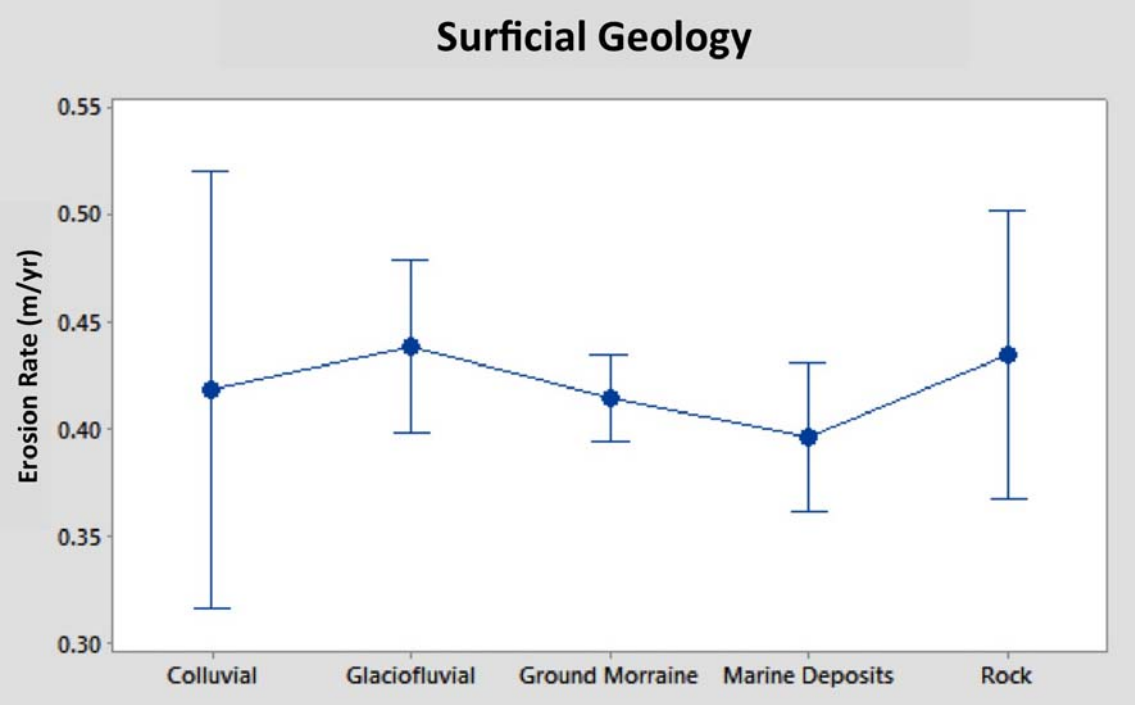

Figure 3.19: Erosion rate plotted against surficial geology. 95 % confidence intervals are shown. p = 0.6.

The ANOVA for terrain gave a p = 0.011 and shows that hilly terrain is associated with higher erosion rates than hummocky terrain. There is no significant difference in erosion rates between hummocky, ridged or flat terrain (Figure 3.20).

Soil drainage along the Minas Basin coastline is only found to be either well drained or imperfectly drained (Figure 3.21). No areas are classified as poorly drained. This factor does not show any correlation to changes in erosion rate (p = 0.338).

Coarse, medium and fine soil textures are all found around the Minas Basin coastline. No correlation was found between soil texture and erosion rate (p = 0.574) (Figure 3.22).

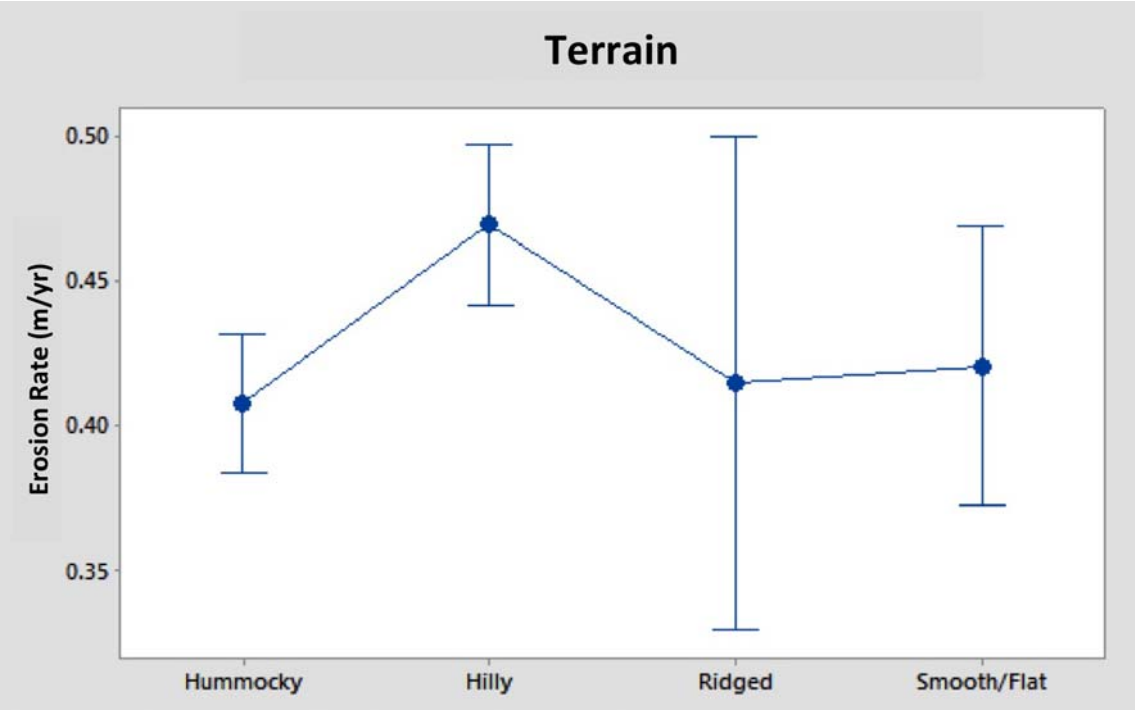

Figure 3.20: Erosion rate plotted against terrain type. 95 % confidence intervals are shown. p = 0.011.

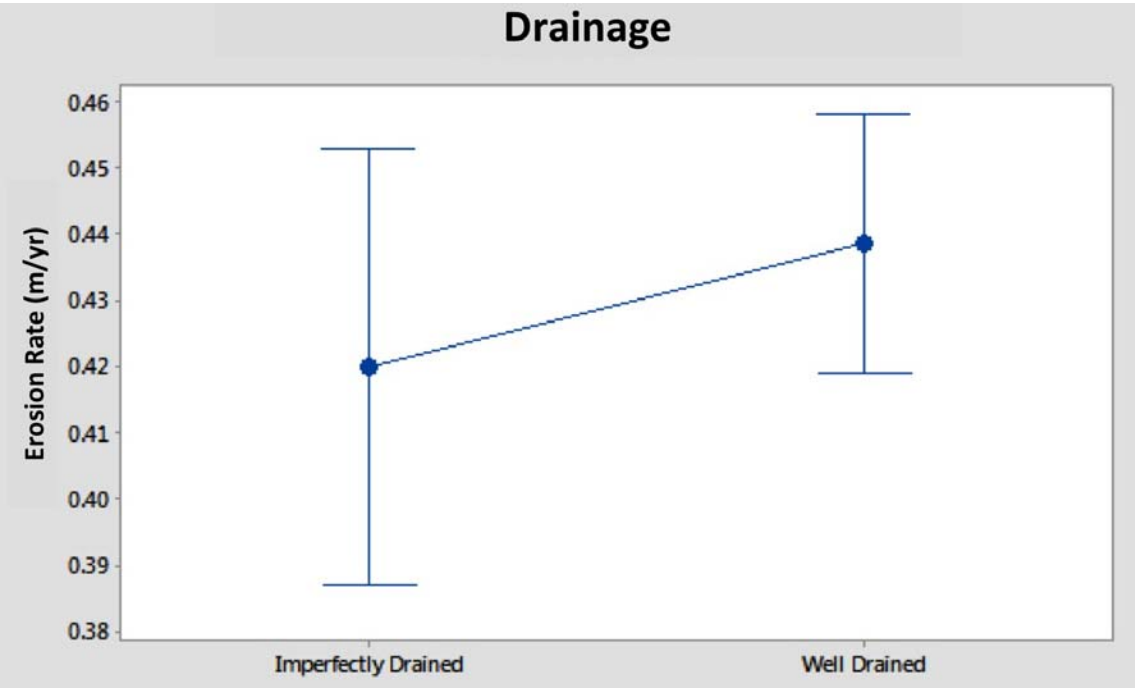

Figure 3.21: Erosion rate plotted against soil drainage. 95 % confidence intervals are shown. p = 0.338.

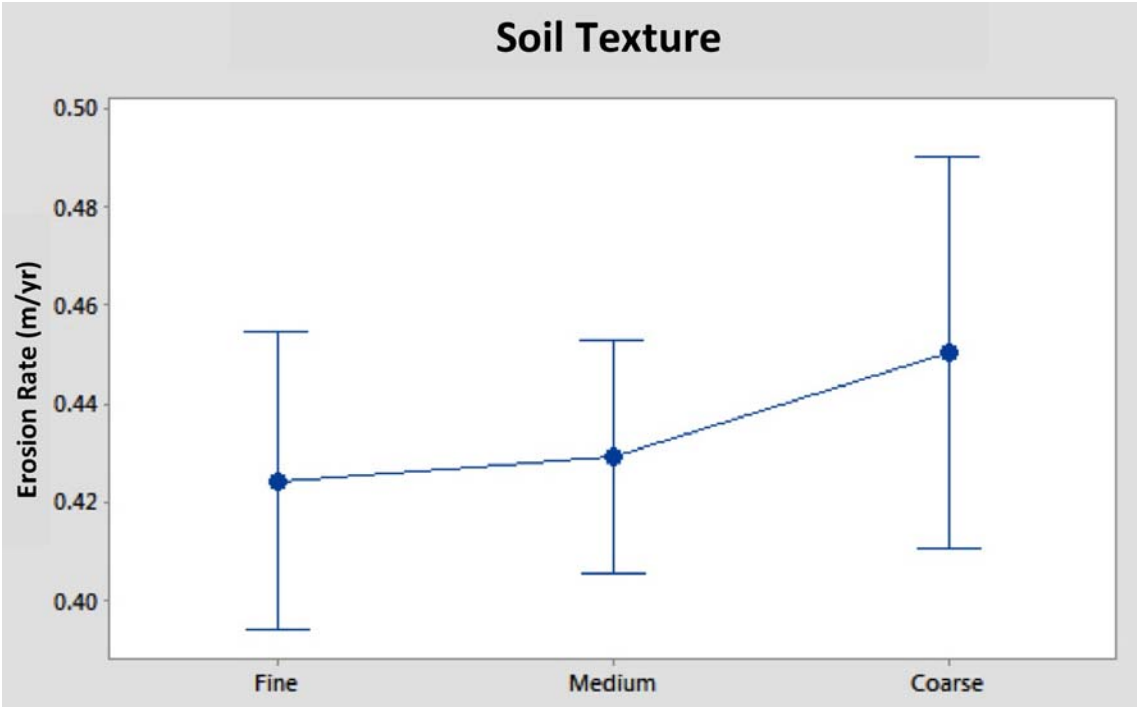

Figure 3.22: Erosion rate plotted against soil texture. 95 % confidence intervals are shown. p = 0.574.

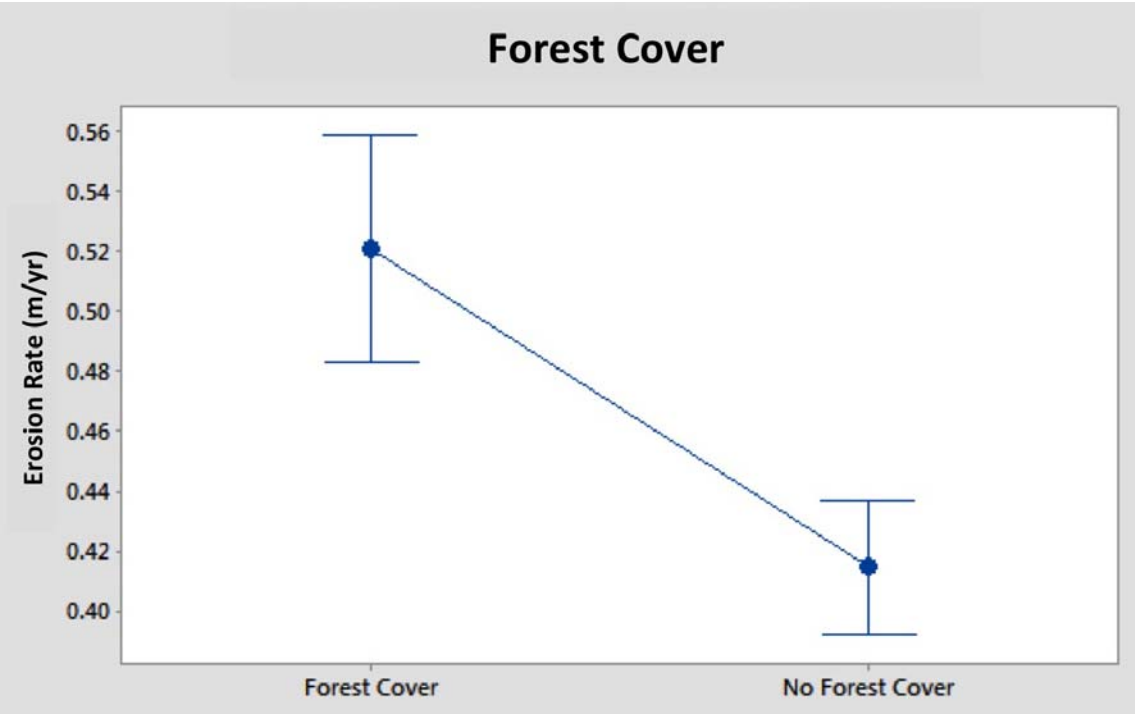

Figure 3.23: Erosion rate plotted against forest cover. 95 % confidence intervals are shown. $p < 0.001$.

Forested areas were found to be significantly correlated with higher erosion rates ($p < 0.001$) (Figure 3.23). Forest cover is defined here as any tree coverage including brush higher than one metre.

Wind fetch values along the coastline also do not explain variations in erosion rates ($p = 0.56$) (Figure 3.24). Elevation, however, does show a weak correlation with erosion rates ($p < 0.001$, $r = 0.35$). Higher erosion rates are found where cliff heights are greater (Figure 3.25).

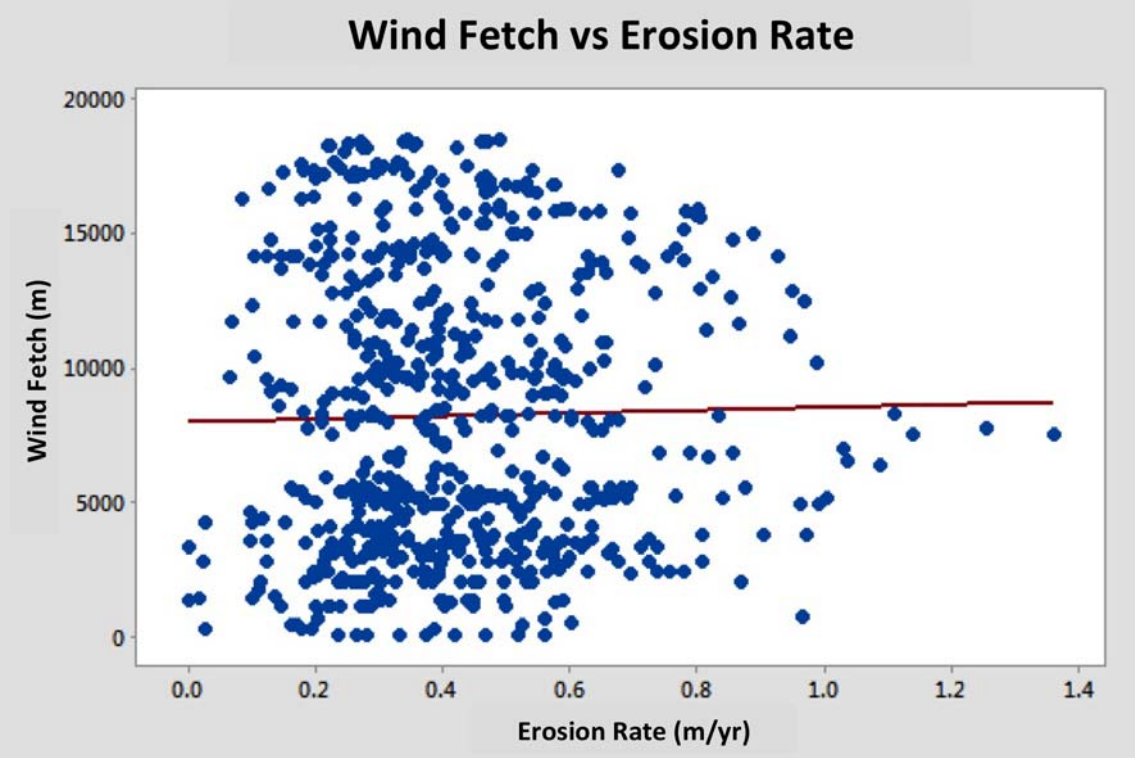

Figure 3.24: Wind fetch plotted with erosion rate. Linear regression line shown in red. p = 0.56, r = 0.023.

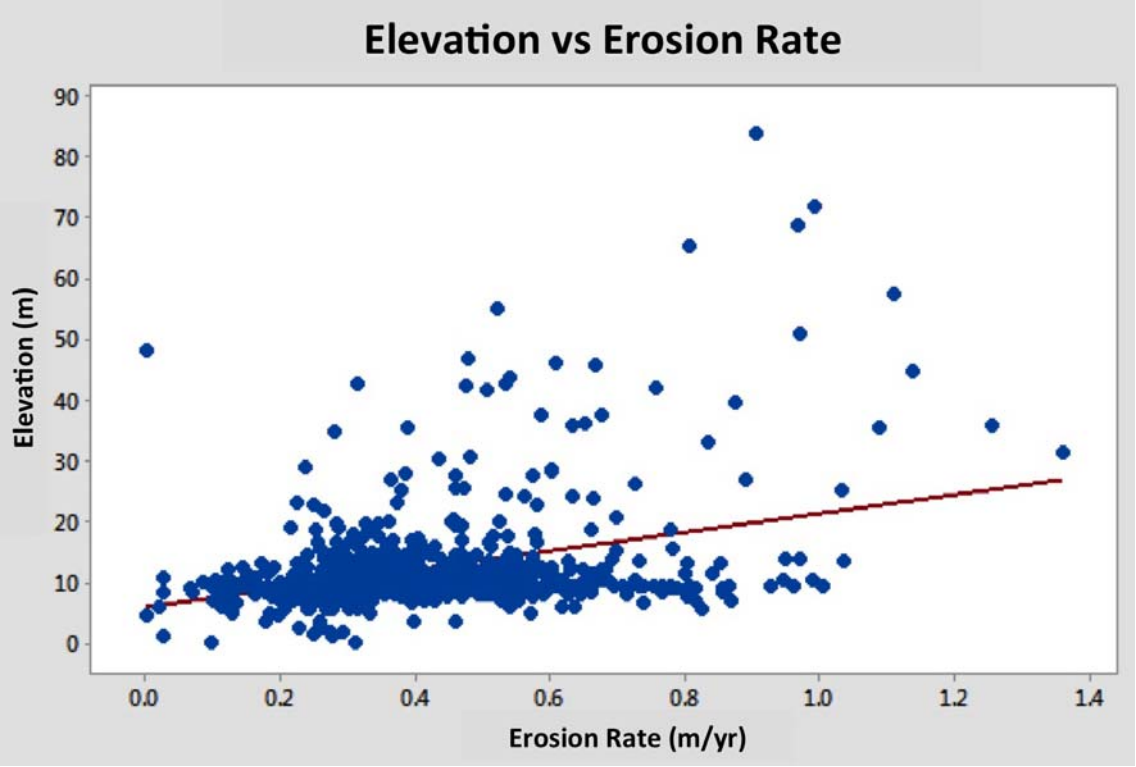

Figure 3.25: Elevation plotted with erosion rate. Linear regression line shown in red. $p < 0.001$ $r = 0.354$.

CHAPTER 4

DISCUSSION

4.1 Errors in Field Methods

The accuracy of the theodolite app method for cliff height measurement was greater for lower cliff heights ($<$ 25 m). This method relies on measuring an elevation angle, y (Figure 2.6) from 15 m out from the cliff base to the top of the cliff. This angle is harder to measure accurately as the cliff height increases.

Also, a small change in elevation angle results in a larger change in the calculated cliff height with tall cliffs compared to shorter cliffs. Table 4.1 shows that a one degree change in the measured elevation angle on a tall (45.2 m) cliff results in a 5.7 m change in calculated cliff height where the same change in elevation angle on a short (2.4 m) cliff only results in a change of 0.4 m in calculated cliff height. A five degree change in elevation angle causes a 46.4 m and 1.8 m change in calculated height respectively.

These examples of error with this method stress the need to make the most accurate measurements possible in the field. This could be achieved by taking multiple elevation angle measurements at sites with tall cliffs. The theodolite application works well as a tool in the field for measuring cliffs smaller than 25 m. Other methods should be used if cliff elevations are known to be higher.

Table 4.1: Changes in calculated cliff height (H) with changes in elevation angle (y) compared for a tall and short cliff

	Tall Cliff	**Short Cliff**
Actual measurement	y = 60° H = 45.2 m	y = 11° H = 2.4 m
1°change in y	y = 61° H = 50.9 m	y = 12° H = 2.8 m
5°change in y	y = 65° H = 91.6 m	y = 16° H = 4.2 m

4.2 Comparison to Previous Work

4.2.1 Linear Erosion

Linear erosion rates measured in this study ranged from 0 m/yr to 1.4 m/yr. The mean erosion rate for the Basin increased from 0.39 to 0.48 m/yr over the two time periods, with an overall mean erosion rate of 0.42 m/yr. *Amos and Long*'s (1980) erosion rates were based on photographs from 1939 to 1964. They reported a maximum erosion rate of 1.6 m/yr along the north shore of the Cobequid Bay and 1.5 m/yr near Five Islands. A mean erosion rate for the Minas Basin was reported to be 0.55 m/yr (*Amos and Long*, 1980). Since the erosion rates throughout the system vary, looking at the mean erosion rate only gives a rough estimate and a baseline for looking at the amount of sediment entering the system. By looking at changes in the 6 smaller sections, a more detailed picture emerges of how and where erosion rates, and thus sediment inputs, are changing with time.

Figure 4.1 shows erosion rates measured along the coastline in each section for the two time periods compared with the rates measured by *Amos and Long* (1980). Data presented in *Amos and Long* (1980) can be found in detail in *Amos and Joice* (1977). Comparing erosion rates for the same locations with the overall rates of the current study using a paired-t test show that the *Amos and Long* (1980) values are significanly higher ($p = 0.006$). It cannot be determined whether these differences are caused by measurement accuracy or are due to the difference time over which they were taken.

Amos and Long (1980) reported negligible erosion rates at Burntcoat Head which is

consistent with the low erosion rates observed in this study. This study provides a much more detailed look at erosion rates along the coastline. This shows how the erosion rates are changing more clearly so risk assessments and management of eroding areas can be focused in the most threatened locations.

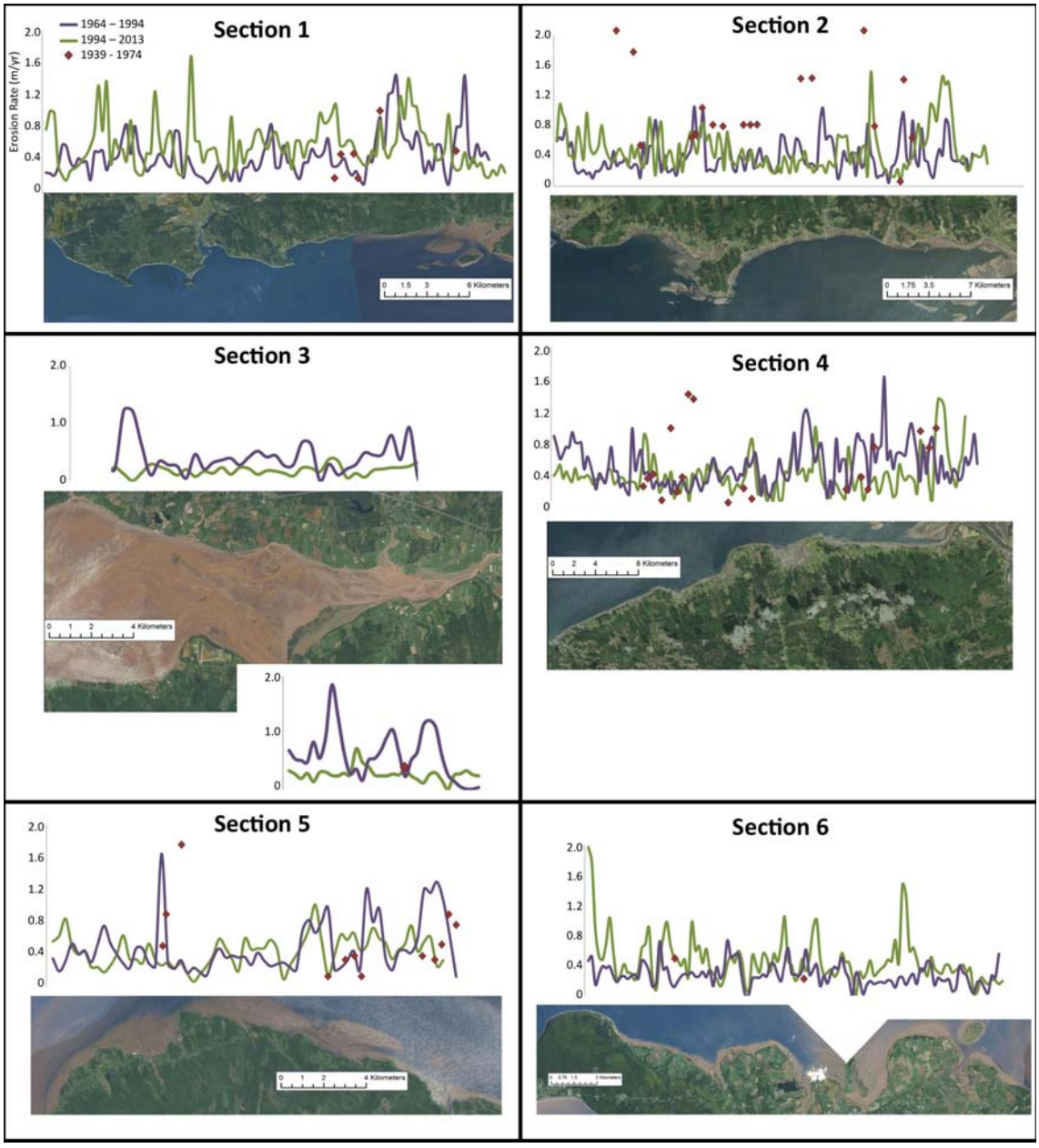

Figure 4.1: Profile graphs of erosion rates (m/yr) for both time periods along each section of coastline.

4.2.2 Volumetric Measurements

The largest input of sediment to the Minas Basin comes from the eroding coastline (*Amos and Long*, 1980). This project provides an updated and more highly resolved estimate of this value, which contributes to the creation of a new sediment budget.

Volumetric inputs ranged from 0 m^3/yr/m to 75.6 m^3/yr/m depending on location. The highest inputs are along the north shore of the Central Basin and the lowest inputs along the western coast of the Southern Bight, the western portion of Cobequid Bay, and areas where coastline elevations are low. The mean input increased from 4.5 m^3/yr/m to 6.3 m^3/yr/m with an overall mean of 5.7 m^3/yr/m for the entire study period. *Amos and Long* (1980) reported a maximum input of 70 m^3/yr/m for a section near Five Islands. They reported overall inputs of 3.09 x 10^6 m^3/yr ($\pm$ 0.93 x 10^6 m^3/yr) using data from 1939 to 1964. This value is approximately three times greater than the 9.0 x 10^5 m^3/yr and 1.3 x 10^6 m^3/yr for time periods one and two respectively from the current study. The number from *Amos and Long* (1980) includes volume input from a section along Cape Split (0.68 x 10^6 m^3/yr), which partially explains the discrepancy in the numbers. This section was not included in the current study due to the degree of distortion in the photographs. *Amos and Long* (1980) did not have directly measured erosion rates from Cape Split. Their sediment input value was calculated using elevation from the site and an erosion rate extrapolated from a section further south along the coast of the Southern Bight.

Having a map that shows the amount of sediment entering from each point along the coastline of the system can help with the further development of sediment models within the Basin. If it is known more precisely where the sediment input points are, the movement of that sediment within the system can be assessed more accurately.

4.2.3 Mass Input

Total sediment mass input had not been calculated for the Minas Basin for cliff inputs before. Although the number calculated here is a rough estimate based on the primary mineral, quartz, of the Wolfville Group that makes up the largest percentage of the coastline (Figure 1.1), it provides an estimate of the mass of sediment provided to the Minas Basin system from coastal erosion sources each year.

Different porosities were taken into account when calculating this mass number. The range of mass values calculated were 2.8, 2.6 and 2.3 megatons for porosities of 0, 8 and 17% respectively. While the different porosities provide mass values within the same order of magnitude, more information on the composition of the material being eroded is necessary to refine the mass input measurement further. These values are a rough estimate, as the actual coastline is not as homogeneous as this calculation assumes.

4.3 Erosion Patterns

Erosion rates throughout the Minas Basin system vary significantly, from areas where little to no erosion is observed to areas where over 1 m of coastline is lost every year. Erosion rates vary over both space and time. Identifying where these rates are highest and where they are increasing allows mitigation efforts to be implemented in the most effective areas. Highest rates are found along the nothern shore of the Basin, especially the western half. Rates are increasing along most of the Minas Basin coastline, except in the Southern Bight, where they are decreasing.

4.3.1 Temporal Patterns

The overall average erosion rate along the Minas Basin coastline increased from 0.39 m/yr to 0.48 m/yr. This is a statistically significant increase. Statistically significant increases in erosion occured in sections 1-5. Section 6 was the only area that showed a significant decrease (Appendix B). Time period 1 of section 6 is shorter than the other sections because aerial photographs were only available in 1977, not 1964 like the other sections. This means that for section 6, erosion rates in time period 1 were only measured over 15 years instead of closer to 30 years. This difference could be the cause of some of the differences in trends observed between section 6 and the other sections.

The largest increase in linear erosion rates is found in Section 3 (Figure 3.2), although the overall erosion rate remains lower than the other sections (Figure 3.3). This section's coastline is dominated by manmade features (dykes) (Figure 3.17b). Erosion rates from there may not be entirely caused by natural processes, but rather by modifications to the dykes. This is further discussed in section 4.3.3.

Increased erosion rates along the north shore of the Central Minas Basin between Parrsboro and Five Islands were also observed. Increases here in linear erosion were smaller than increases observed in section 3, however this section of the coastline is composed of large cliffs, so the increase in overall sediment input to the system is much larger here (Figure 3.11).

4.3.2 Spatial Patterns

The north shore of the entire Basin showed higher erosion rates than the south shore. The southern shore has higher rates to the eastern side and the rates decrease westward, with the exception of coastline directly west of Walton River. The lowest overall rates are observed along the coast of the Southern Bight, increasing closer to Cape Split and along the western coast of Cobequid Bay.

Physical factors such as bedrock geology, surficial geology, forest cover, exposure to wind and waves and others vary along the coast of the Minas Basin. Factors with data available were assessed to explore if any physical characteristics of the coastline can explain the observed variation in erosion rates. Since many of the physical factors, such as bedrock and surficial geology would not have changed over the study period and there are few data available on any that may have changed, such as forest cover, the temporal changes were not taken into account and the overall rates for the entire study period were used.

4.3.3 Dykes

The construction of dykes along the Minas Basin coast allowed early French settlers to turn marshlands into fertile agricultural land. Dykes are vulnerable to erosion and need to be maintained in order to continue to protect farmland and properties behind them (*Asiedu*, 2013).

During storm events, dykes can be breached, leading to flooding of the lowlands behind them. Storms in 1869, 1893, 1923, 1927 and 1931 breached dykes and flooded dykelands near Truro (*Asiedu*, 2013). Modifications were made through provincial and federal government programs beginning in 1947 to protect dykelands from flooding during storms

(*NSDAM*, 1987). Major renovations were made to the dyke system from 1967 to 1970. These modifications, along with improved maintenance meant less damage occurred during a large storm in 1977 (*Robinson et al.*, 2004).

The Canadian Federal Government stopped assisting with dyke maintenance in 1970, shifting responsibility to the provincial government and landowners. Now, dyke maintenance is not completed annually, but it depends on dyke condition. As of 2012, 60 km of dykes in Nova Scotia are located below the high tide line and considered to be at serious risk (*Asiedu*, 2013). Hurricane Bill caused erosion and a breach in a dyke on the Noel Shore in 2009 (*Van Proosdij*, 2009). Dykes near Truro also breached and caused major flooding in 2012.

Eroding foreshore marshes put dykes more at risk. Foreshore marshes protect the coastline by dissipating wave energy (*Möller et al.*, 1999). Marshes can often be the difference between protection from storm surges and severe dykeline damage from storm events. This was seen along the Noel Shore in 2009, where dykes were only breached where no foreshore marsh was present (*Van Proosdij*, 2009).

Eroding and breaching of dykes can provide sediment to the system. However, because dykes are maintained, erosion rates in these areas may not reflect natural erosion rates. Dyke elevations are low and therefore sediment input from dyked coastlines is minimal compared to inputs from cliffed coastlines.

4.4 Causes of Variations in Erosion Rate

Several physical variables in the environment were assessed to determine if there was any correlation between them and erosion rates along the coast. Past studies state that erosion rates are high in the Minas Basin due to the friable sandstone along the coast (*Amos and Long*, 1980; *Desplanque and Mossman*, 2004), however, a range of erosion rates from very small to the largest are found where sandstone is present. Its friable nature does make the coastline prone to erosion, but it is not the only factor in determining erosion rates.

Some single characteristics within a given physical factor showed correlation with higher erosion rates than other characteristics. The Parrsboro, North Mountain and McCoy

bedrock formations were associated with higher erosion rates than the Wolfville formation (Figure 3.18). Hilly terrain showed higher erosion rates than hummocky terrain, but other types of topography showed no significant affect on erosion rate.

Forest cover was one physical factor that has a significant affect on erosion rates. Areas where vegetation was present are associated with higher erosion rates. Roots of larger plants and trees may aid in breaking apart friable cliff faces. Locations of forested areas in relation to other factors may contribute to some of the correlation with erosion rates. These interactions were not explored.

Sections of coastlines located behind salt marshes predominantly had low erosion rates (Figure 3.17). Low erosion rates were also found in areas without the presence of salt marshes, so they can not be used soley as indicator of coastal erosion rate. Although they help to protect the coastline behind them, salt marshes are present in areas sheltered from high wave action (*Davidson-Arnott et al.*, 2002) which likely also contributes to the low erosion rates.

4.4.1 Elevation

Elevation of the coastline shows weak correlation with erosion rate. Where the height of the coastline is larger, the erosion rates are larger. This is consistent with the theory that landscapes are eroded primarily by slope movement (*Willet*, 1999) and that sediment flux increases with increased gradient (*Dietrich et al.*, 2013; *Roering et al.*, 1999). With extremely steep landscapes, the rate of erosion cannot be predicted based on the slope angle because the relationship between slope of the landscape and sediment transport becomes strongly non-linear (*Roering et al.*, 1999; *Willet*, 1999). Steep cliffed coastlines often erode due to failures triggered by other events (*Young et al.*, 2009), as undercutting at the base of a cliff occurs, mass movement by slumps and rock falls becomes more common (*Emery and Kuhn*, 1982). This is also consistent with what is observed in the Minas Basin, where areas with steep cliff faces are known to lose large sections over short time scales from days to seasons. The erosion rate over a given time period can be affected, as these rapid events mean that erosion rates in these cliffed areas are not constant over time. This could help explain the lack of correlation between physical factors of the coastline and erosion rates.

The notable exception to this is the area around Burntcoat Head. This area is lined with steep cliffs but relatively low erosion rates (0 – 0.5 m/yr) were measured here, consistent with negligible values observed by Amos and Long (1980).

4.4.2 Wind Fetch

Amos and Long (1980) cited degree of cliff exposure to wave attack as a leading cause of erosion along the coastline of the Minas Basin. While it is known that waves can eat away at coastlines and undercut cliffs leading to rock falls (*Collins and Sitar*, 2008; *Desplanque and Mossman*, 2004; *O'Carroll*, 2010), there is little information on wave propagation in the Minas Basin. *Li et al.* (2015) modeled maximum significant wave height in the Bay of Fundy showing that the effect of waves decreases to the northeast of the Bay. Wave stress is shown to have an effect over tidal dominance along the coast in the Southern Bight, and some mixed tide and wave stress can be seen on the western part of the north shore of the Central Minas Basin. However, they state that no wave data were available for the head of the Minas Basin. Without detailed descriptions of the wave propagation in the Minas Basin, no definitive connection can be drawn to areas where waves reach the shoreline and rates of erosion along the coast.

The Minas Basin is sheltered from the swells of the outer Bay of Fundy and most of the waves are locally wind generated (*Amos and Long*, 1980). This thesis looked at wind fetch as an indicator of wave propagation. Wind fetch is distance that wind can blow unobstructed over water. Therefore, where there is a larger wind fetch, larger wind–generated waves can develop, which could lead to increased coastal erosion where they interact with the coastline (*Rohweder et al.*, 2012).

Amos and Long (1980) note that the dominant direction of wave propagation would correspond to the dominant south–west wind direction and could explain the higher erosion rates found along the northern shore of the Basin. The wind fetch model created here (Figure 3.16), shows that the largest wind fetches, weighted with the percent of time the wind blows in each direction, do interact with the coastline along most of the nothern shore of the Minas Basin, where higher erosion rates are found. However, when these wind fetch values are compared with the erosion rates along the entire Basin coastline, no statistcally significant correlation is observed (Figure 3.24). The largest wind fetch interacts with the

coastline at the northern shore of Cobequid Bay, which is dominated by dykes. Since these areas are maintained, erosion rates here may not reflect the impact wave propagation has on the coastline.

This assessment of wind fetch and associated wave attack does not take into account the timing of the wind with the tides. In an environment with such a large tidal range, this is a relationship that needs to be explored further. Waves only attack the coastline along the Minas Basin when the cliff bases are innundated. This happens in some areas at high tide. Also, when the foreshore waters are much deeper at high tide, more wave energy can reach the shoreline compared to when water is shallower or mud flats are exposed (*Desplanque and Mossman*, 2004). In areas where there are no cliffs, high tides corresponding with increased wave activity during a storm can also lead to dyke breaching, resulting in inland flooding.

The cliffs along the Minas Basin can be innundated up to 2 m in some areas at high tide and this innundation has been cited as a cause of erosion in the Minas Basin (*Amos and Long*, 1980). With access to more detailed LiDAR based digital elevation models, a map could be created to determine the extent of cliff innundation along the entire coastline to test for correlation to erosion rates and to identify areas that may be more prone to wave undercutting and erosion. Being able to compare the wind fetch values to current patterns could also help to resolve wave propagation in the Minas Basin, as the locations where currents move against highest wind fetch would produce higher waves (*Greenberg*, 1985).

4.4.3 Future Influences

The Minas Basin is a dynamic and ever-chaging system. With growing impacts from climate change, future changes to this system that may influence the rate of erosion can not be ignored. Present day sea level in the Minas Basin is increasing at a rate of 3.0 mm/yr due to the combined effect of eustatic global sea level rise and crustal subsidence (*Gehrels et al.*, 2004). Crustal subsidence, based on measurements from a Truro GPS station, accounts for 1.29 mm/yr of the total increase (*James et al.*, 2014). Sea level could rise at much as 75 cm in the next 100 years based on the most extreme climate scenarios (*James et al.*, 2014). Higher sea level means that more of the coastline would be innundated at high tide and more wave energy could therefore reach the coast, possibly causing higher

erosion rates. There is also a greater likelihood of coastline defence breaches and more frequent flooding in low lying areas with higher sea levels. It is also predicted that the strength and frequency of storm events could increase due to anthropogenic climate change (*Jones et al.*, 2007; *O'Carroll*, 2010). These changes could have affects on the erosion rates in the Basin.

A positive storm tide is a large increase in water levels accompanying a coastal storm (*Desplanque and Mossman*, 2004). This happens when a surge from a storm coincides with high tide. The results in terms of coastal flooding and erosion can be more catastrophic if storm landfalls coincide with very high tides. Events like this have happened, most notably the Saxby Tide in 1869, the Storm Tide of 1759 and the Groundhog Day Storm of 1976. During each of these events the tide rose several meters above the astronomically predicted levels, breaching dykes and heavily eroding the coastline (*Desplanque and Mossman*, 2004). Although *Desplanque and Mossman* (2004) state that the probabilty of events such as these are relatively low, with known increases in sea level and prediced increases in storminess, these events could occur more often, causing more catastrophic erosion events and further increases to erosion rates.

4.5 Sediment Accumulation

There has been disagreement over whether or not the Minas Basin system is in hydrodynamic equilibrium in terms of current speeds and sediment bed texture. *Emery and Uchupi* (1972) describe sediment dynamics and transport rates in the Bay of Fundy based on equilibrium in the system, and *Amos* (1978) states that sediment texture is in equilibrium with maximum bottom currents. *Amos and Long* (1980) note that there is no relationship between current speed and suspended sediment concentration in the Minas Basin. *Gelati* (2012) also found that the bed sediment texture in the Minas Basin is generally finer than expected based on maximum tidal bed shear stress. Sediment supply has been suggested as the cause of this discrepancy (*Gelati*, 2012).

Sediment volume inputs from this study are significantly lower than the inputs reported by *Amos and Long* (1980). This should bring the system closer to hydrodynamic equilibrium despite what *Gelati* (2012) observed.

If all the sediment input from the coastline remains in the basin and was evenly distributed, it would accumulate at a rate of about 1 mm/yr. This value is equivalent to what is observed within the Basin (*Amos and Long*, 1980), meaning sediment is not being exported from the system. *Li et al.* (2015) also show that about 2 megatons of sediment is brought in from the outer bay through the Minas Passage every year, which is equivalent to *Amos and Long*'s (1980) observations and comparable to coastal erosion inputs.

The Minas Basin, therefore, acts as a sediment trap, with net influxes from the outer bay and coastal erosion collecting in the Basin. The magnitude of these inputs overwhelm the system's ability to remove the finer grains, which would be expected based on the current speeds observed. This pushes the bed sediment texture out of equilibrium with the maximum bottom currents. When a system is not in hydrodynamic equilibrium, simple conclusions between changes in current speed and changes in sediment texture cannot be drawn. This means that more complex methods would need to be used when predicting changes that tidal turbine use may have on sediment bed composition. However, if sediment bed texture is dominated by inputs and not by bottom current speeds, changes from tidal turbine emplacement would be minimal.

4.6 Recommendations for Future Work

The volumetric inputs of sediment from coastal erosion to the Minas Basin system have been measured in greater detail than the previous sediment budget provided. Given access to DEM models created by LiDAR data, these volumetric inputs could be resolved even further. More detailed DEM data would also allow for a map of cliff innundation sites to be created which could be an important cause of higher erosion rates along parts of the coastline.

Creating a wave propagation model to combine with the wind fetch model and cliff innundation information could provide more insight into the causes of higher erosion rates in certain areas and help to define areas of the coastline are most at risk.

To further improve sediment dynamic and texture models in the Minas Basin, information on sediment inputs should be included. Volumetric inputs provided in this study

allow for more detailed constraints on the location and amount of sediment inputs from this dominant source. Information on grain size of coastal erosion inputs should also be included in these models.

Sediment inputs from other sources, such as river inputs and salt marsh erosion should be assessed along with sinks of sediment in the area in order to complete an updated sediment budget for the Minas Basin system.

CHAPTER 5

CONCLUSIONS

The high energy of the Minas Basin system has made this area a focus for research on in-stream tidal power generation. In order to comprehend the impact of this technology on the Minas Basin, a full understanding of all components in the system is required. A sediment budget for the Minas Basin has not been completed since the 1970's and it was based on a limited understanding of the sediment input from coastal erosion sources. This study provides updated measurements of this sediment source as well as detailed erosion rates along the entire coastline.

GIS methods were used to measure continuous linear erosion and volumetric sediment input rates along the entire coastline of the Minas Basin. Current erosion rates along the coast range from 0 - 1.4 m/yr with a mean of 0.42 m/yr. Highest erosion rates are found along the northern shore of the Central Minas Basin. Erosion rates have increased from time period 1 (1964 - early 1990's) to time period 2 (early 1990's - 2013) in almost all areas of the system, with the exception of the Southern Bight.

Total inputs of sediment to the Minas Basin from coastal erosion sources have increased from 9.0 x 10^5 m^3/yr to 1.3 x 10^6 m^3/yr over the time periods studied with a average of 2.6 megatons of sediment entering the Basin every year. The dominant source of sediment input comes from the cliffs along northern shore of the Central Minas Basin between Five Islands and Parrsboro where high linear erosion rates are found and the elevation of the coastline is high.

The volume of sediment entering the system, although smaller than suggested by *Amos*

and Long (1980), provides enough sediment to the Basin to overwhelm the system's ability to remove it. This is in agreement with *Gelati*'s (2012) observations that sediment bed texture is finer than expected based on maximum tidal bed shear stress, suggesting the system is not in hydrodynamic equilibrium. This means that predicting changes in sediment texture due to emplacement of tidal turbines is not possible based on current speeds alone.

Elevation was one physical factor examined that showed some correlation with erosion rate. Erosion rates tend to be higher where the height of the cliffs along the coastline is higher. Areas with forest cover show higher erosion rates, where as soil drainage, soil texture, and surficial geology show no relationship with erosion rates along the coast. This highlights the complex processes at work in the system and the need to look at other marine processes that could be used as indicators of where increased erosion rates will occur in the future.

Results from this study not only help update the sediment budget for the Minas Basin, but also can help in the focus of coastal erosion mitigation efforts and can be used to further the understanding of the sediment dynamics in this system. By better constraining the main sediment input to this system, cliff sources can be added to sediment texture models to better resolve the transport processes and provide a baseline from which to predict possible changes from extracting tidal power.

APPENDIX A

FIELD CLIFF HEIGHT CALCULATIONS

Example of field measurements from one site:

X = 65° Z = 2.5° Y = 11° a = 15 m

Example of cliff height calculation from above field measurements:

Finding K
(Supplementary angles)

$$180° - X = K \tag{A.1}$$
$$180° - 65° = 115°$$
$$K = 115°$$

Finding M
(Sum of interior angles)

$$180° - K - Z = M \tag{A.2}$$
$$180° - 115° - 2.5° = 62.5°$$
$$M = 62.5°$$

Finding F
(Supplementary angles)

$$180° - M = F \tag{A.3}$$
$$180° - 62.5° = 117.5°$$
$$F = 117.5°$$

Finding L
(Sum of interior angles)

$$180° - F - (Y - Z) = F \tag{A.4}$$
$$180° - 117.5° - (11° - 2.5°) = 44.8°$$
$$L = 54°$$

Finding b
(Law of Sines)

$$\frac{a}{\sin L} = \frac{b}{\sin(Y - Z)} \tag{A.5}$$
$$\frac{15}{\sin 54°} = \frac{a}{\sin 8.5°}$$
$$b = 2.74\,\text{m}$$

Finding h
(Law of Sines)

$$\frac{h}{\sin X} = \frac{b}{\sin 0°} \tag{A.6}$$
$$\frac{h}{\sin 65°} = \frac{b}{\sin 90°}$$
$$b = 2.4\,\text{m}$$

APPENDIX B

COMPARISONS IN EROSION RATE AND VOLUMETRIC INPUT BY SECTION

Results from ANOVA done comparing the overall erosion rates and volumetric input rates between each of the 6 section assessed.

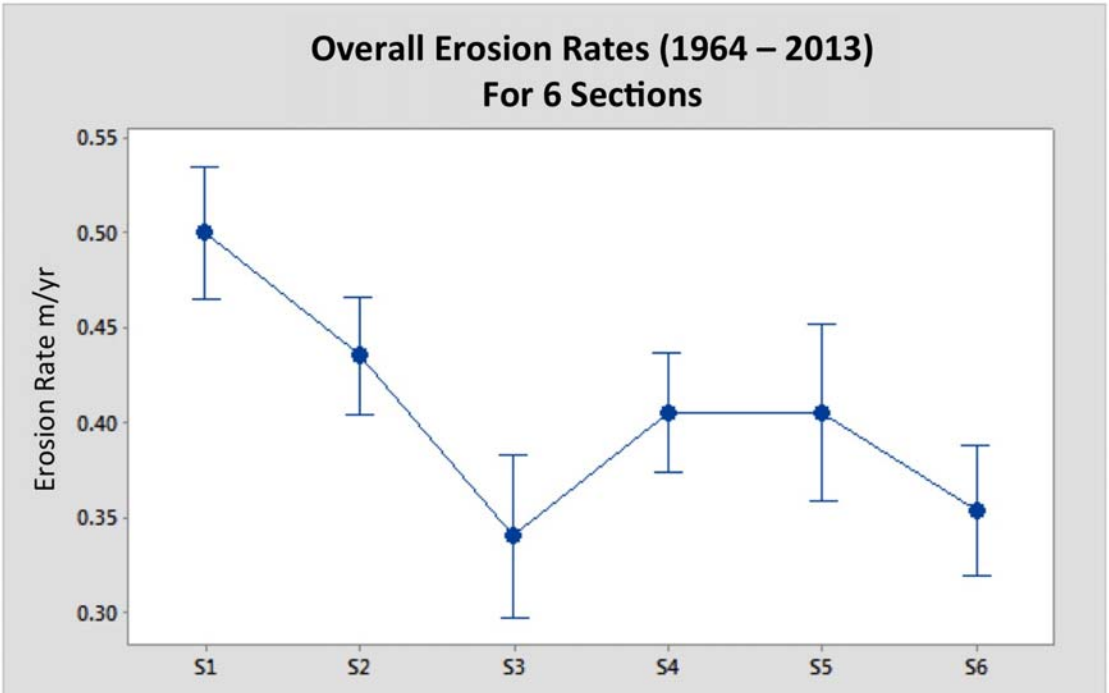

Figure B.1: Points show mean erosion rate overall (1964 - 2013) for each section. Lines are 95 % C.I.

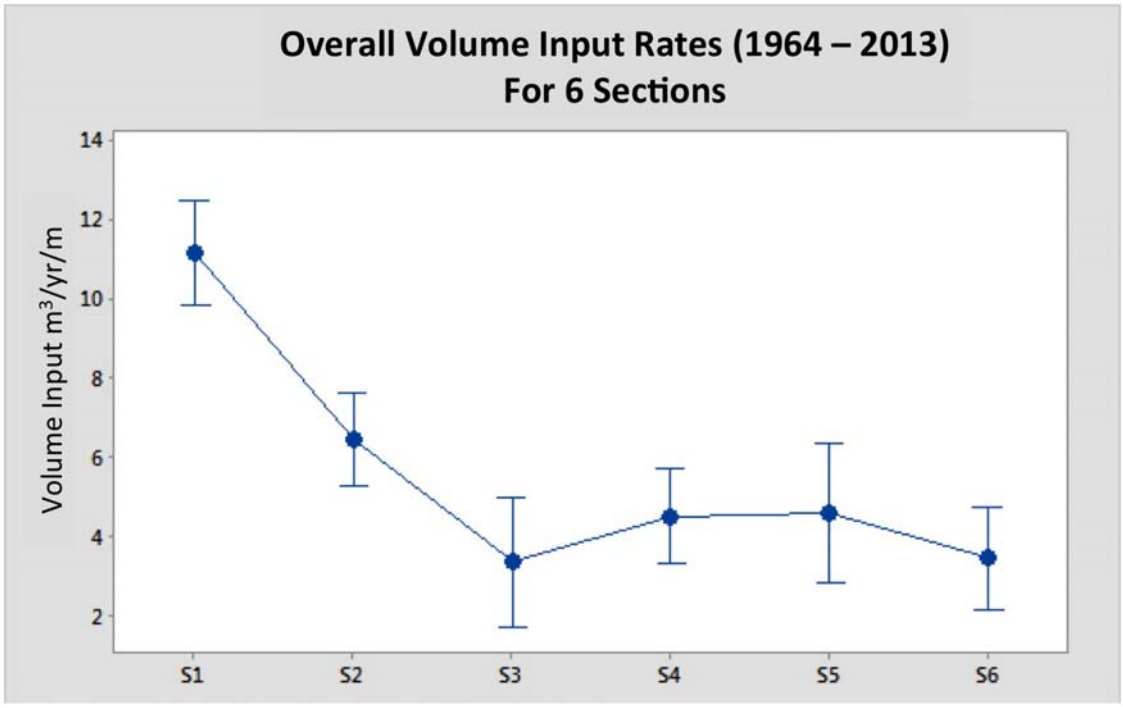

Figure B.2: Points show mean volume input rate overall (1964 - 2013) for each section. Lines are 95 % C.I.

BIBLIOGRAPHY

Amos, C., The post glacial evolution of the Minas Basin, N.S. a sedimentological interpretation, *Journal of Sedimentary Petrology*, *48*, 965–982, 1978.

Amos, C., and G. Joice, The sediment budget of the Minas Basin, Bay of Fundy, N.S., *Bedford Institute of Oceanography, Dartmouth, Nova Scotia, Canada*, 1977.

Amos, C., and B. Long, The sedimentary character of the Minas Basin, Bay of Fundy, *Proc. Coastlines Canada Conf., Halifax, NS*, 1980.

Armaroli, C., P. Ciavola, Y. Balouin, and M. Gatti, An integrated study of shoreline variability using GIS and ARGUS techniques, *Journal of Coastal Research: Special Issue*, *39*, 473–477, 2006.

Asiedu, G., Citizen's perception of values associated with dykes and dykelands: the case of Nova Scotia, *unpublished Masters Thesis: Dalhousie University*, 2013.

Benumof, B., and G. Griggs, The dependence of seacliff erosion rates on cliff material properties and physical processes: San Diego county, California, *Shore and Beach*, *67*, 1167–1178, 1999.

Bird, E., Coasts, *Science*, *166*, 1969.

Boak, J., and I. Turner, Shoreline definition and detection, a review, *Journal of Coastal Research*, *21*, 2005.

Brock, J., and S. Purkis, The emerging role of lidar remote sensing in coastal research and resource management, *Journal of Coastal Research: Special Issue*, *53*, 1–5, 2005.

Buffington, J., and D. Montgomery, Effect of sediment supply on surface textures of gravel-bed rivers, *Water Resources Research*, *35*, 3523–3530, 1999.

Butler, K., G. Fader, E. Kosters, T. Milligan, D. Muschenheim, R. Parrott, and D. Van Proosdij, Greater Bay of Fundy: what we need to know and do in order to become good stewards, *Atlantic Geoscience Society unpublished report*, p. 4p, 2006.

Byrnes, M., R. McBride, and M. Hiland, Accuracy standards and development of a national shoreline change database, *Proceedings of the Coastal Sediments*, pp. 1027–1042, 1991.

Carr, A., Cartographic record and historical accuracy, *Geography*, *47*, 135–144, 1962.

Chaaban, F., H. Darwishe, Y. Battiau-Queney, B. Louche, E. Masson, J. Khattabi, and E. Carlier, Using arcgis modelbuilder and aerial photographs to measure coastline retreat and advance: North of France, *Journal of Coastal Research*, *28*, 2012.

Collins, B., and N. Sitar, Processes of coastal bluff erosion in weakly lithified sands, Pacifica, California, USA, *Geomorphology*, *97*, 483–501, 2008.

Davidson-Arnott, R., D. van Proosdij, J. Ollerhead, and L. Schostak, Hydrodynamics and sedimentation in salt marshes: examples from a macrotidal marsh, Bay of Fundy, *Geomorphology*, *48*, 209–231, 2002.

Davis, M., Geomorphic shoreline classification of Prince Edward Island, *Atlantic Climate Adaption Solutions Association*, 2011.

Desplanque, C., and D. Mossman, Tides and their seminal impact on the geology, geography, history and socio-economics of the Bay of Fundy, eastern Canada, *Atlantic Geology*, *40*, 1–130, 2004.

Dietrich, W., D. Bellugi, L. Sklar, J. Stock, A. Heimsath, and J. Roering, Geomorphic transport laws for predicting landscape form and dynamics, *Prediction in Geomorphology, the American Geophysical Union*, 2013.

Dolan, R., B. Hayden, and S. May, Erosion of US shorelines, 1983.

Emery, K., and G. Kuhn, Sea cliffs: their processes, profiles and classification, *Geological Society of America Bulletin*, *93*, 644–654, 1982.

Emery, K., and E. Uchupi, Western North Atlantic Ocean: topography, rocks, structure, water, life and sediments, *The American Association of Petrolium Geologists*, 1972.

Garrett, C., Tidal resonance in the Bay of Fundy and Gulf of Maine, *Nature*, *238*, 441–443, 1972.

Gehrels, W., G. Milne, J. Kirby, R. Patterson, and D. Belknap, Late Holocene sea-level changes and isostatic crustal movements in Atlantic Canada, *Quaternary International*, *120*, 79–89, 2004.

Gelati, S., Modeling the impact on sediment texture of large-scale tidal power in the Bay of Fundy, *unpublished masters thesis: Dalhousie University*, 2012.

Greenberg, D., A review of the physical oceanography of the Bay of Fundy, 1985.

Jackson, C. W., C. R. Alexander, and D. M. Bush, Application of the AMBUR R package for spatio-temporal analysis of shoreline change: Jecyll Island, Georgia, USA, *Computers and Geosciences*, *41*, 199–207, 2012.

James, T., J. Henton, L. Leonard, A. Darlington, D. Forbes, and M. Craymer, Relative sea–level projections in canada and the adjacent mainland United States, *Geological Survey of Canada*, 2014.

Jones, P., et al., Observations: surface and atmospheric climate change, *In Climate Change 2007: The Physical Science Basis. Contribution of Working Group I to the Fourth Assessment Report of the Intergovernmental Panel on Climate Change*, pp. 235–336, 2007.

Kettanah, Y. A., M. Y. Kettanah, and G. D. Wach, Provenance, diagenesis and reservoir quality of the Upper Triassic Wolfville Formation, Bay of Fundy, Nova Scotia, Canada, *Geological Society of London: Special Publications*, *417*, 2013.

Larinov, G., N. Bushueva, Z. Dobrovol'skaya, S. Krasnov, and L. Litvin, Effect of gravity on the erosion of model samples, *Eurasian Soil Science*, *48*, 759–763, 2015.

Li, M., Modeling sediment mobility in the Bay of Fundy: how strong the currents are and how often sediment gets transported, *Ocean and Ecosystem Science Seminar Series, Bedford Institute of Oceanography*, 2011.

Li, M., J. Shaw, B. Todd, V. Kostylev, and Y. Wu, Sediment transport and development of banner banks and sandwaves in an extreme tidal system: Upper Bay of Fundy, Canada, *Continental Shelf Research*, 2013.

Li, M., C. Hannah, W. Perrie, C. Tang, R. Prescott, and D. Greenberg, Modelling seabed shear stress, sediment mobility and sediment transport in the Bay of Fundy, *Canadian Journal of Earth Science*, *52*, 757–775, 2015.

Lim, M., N. Rosser, D. Petley, and M. Keen, Quantifying the controls and influence and tide and wave impacts of coastal rock cliff erosion, *Journal of Coastal Research*, *27*, 2011.

Longwell, C., R. Flint, and J. Sanders, Physical geology, 1969.

Martinez, R., R. Silva, and E. Mendoza, Identification of coastal erosion causes in Matanchen Bay, San Blas, Nayarit, Mexico, *Journal of Coastal Research: Special Issue*, *71*, 93–99, 2014.

Methratta, E., and J. Link, Associations between surficial sediments and groundfish distributions in the Gulf of Maine–Georges Bank region, *North American Journal of Fisheries Management*, *26*, 473–489, 2006.

Möller, I., T. Spencer, J. French, D. Leggett, and M. Dixon, Wave transformation over salt marshes: a field and numerical modelling study from North Norfolk, England, *Estuarine, Coastal and Shelf Science*, *49*, 411–426, 1999.

Moore, L., B. Benumof, and G. Griggs, Coastal erosion hazards in Santa Cruz and San Diego, *Journal of Coastal Research: Special Issue*, *28*, 121–139, 1999.

Morton, R., M. Leach, J. Paine, and M. Cardoza, Monitoring beach changes using gps surveying techniques, *Journal of Coastal Research*, *9*, 702–720, 1993.

NSDAM, (Nova Scotia Department of Agriculture and Marketing), Maritime dykelands: the 350 year struggle, *Province of Nova Scotia*, 1987.

O'Carroll, S., Coastal erosion and shoreline classification in Stratford, Prince Edward Island, *Atlantic Climate Adaptation Solutions Association*, 2010.

Owens, E., Coastal environments: oil spills and clean up programs in the Bay of Fundy, *Fisheries and Environment Canada: Economic and Technical Report*, 1977.

Parker, M., M. Westhead, and A. Service, Ecosystem overview report for the Minas Basin Nova Scotia, *Prepared for Ocean and Habitat Branch Maritimes Region, Fisheries and Oceans Canada*, 2007.

Pepe, G., and G. Coutu, Beach morphology change study using ArcGIS spatial analyst, *Middle States Geographer*, *41*, 91–97, 2008.

Pye, K., and S. Blott, Spatial and temporal variations in soft cliff erosion along the Holderness coast, East Riding of Yorkshire, UK, *Journal of Coastal Conservaion*, *19*, 785–808, 2015.

Raju, D., K. Santosh, J. Chandrasekar, and T. Tiong-Sa, Coastline change measurement and generating risk map for the coast using geographic information system, *The International Archives of the Photogrammetry, Remote Sensing and Spatial Information Sciences*, *8*, 492–497, 2010.

Revell, D., R. Battalio, B. Spear, P. Ruggerio, and J. Vandever, A methodology for predicting future sea level rise on the California coast, *Climatic Change*, *109*, 251–276, 2011.

Robinson, L., Marine erosive processes at the cliff foot, *Marine Geology*, *23*, 257–271, 1977.

Robinson, S., D. Van Proosdij, and H. Kolstee, Change in dykeland practices in agricultural salt marshes in Cobequid Bay, Bay of Fundy, *BoFEP Conference Proceedings*, 2004.

Roering, J., J. Kirchner, and W. Dietrich, Evidence for nonlinear diffusive sediment transport on hillslopes and implications for landscape morphology, *Water Resources Research*, *35*, 853–870, 1999.

Rohweder, J., J. Rogala, B. Johnson, D. Anderson, S. Clark, F. Chamberlin, D. Potter, and K. Runyon, Application of wind fetch and wave models for habitat rehabilitation and enhancement projects: 2012 update, *Contract reposrt prepared for U.S. Army Corps of Engineers' Upper Mississippi River Restoration - Environmental Management Program.*, p. 52, 2012.

Ruhl, M., Grain size analysis of sediments from the Minas Basin, Nova Scotia - controls of erosion on seabed sediment texture, *unpublished honours thesis, Dalhousie University*, 2016.

Stafford, D., and J. Langfelder, Air photo survey of coastal erosion, *Photogrammetric Engineering*, *37*, 565–575, 1971.

Sunamura, T., A relationship between wave-induced cliff erosion and erosive forces of waves, *The Journal of Geology*, *85*, 613–618, 1977.

Van Proosdij, D., Assessment of flooding hazard along the highway 101 corridor near Windsor, N.S. using LIDAR, *submitted to the Nova Scotia Department of Transportation and Infrastructure Renewal*, 2009.

Vann Jones, E., N. Rosser, M. Brain, and D. Petley, Quantifying the environmental controls on erosion of a hard rock cliff, *Marine Geology*, *363*, 230–242, 2015.

Willet, S., Orogeny and orography: the effects of erosion on the structure of mountain belts, *Journal of Geophysical Research*, *104*, 28957–28981, 1999.

Woolard, J., and J. Colby, Spatial characterization, resolution and volumetric change of coastal dunes using airborne LiDAR: Cape Hatteras, North Carolina, *Geomorphology*, *48*, 269–287, 2002.

Young, A., R. Guza, R. Flick, W. O'Reilly, and R. Gutierrez, Rain, waves and short term evolution of composite sea cliffs in Southern California, *Marine Geology*, *267*, 1–7, 2009.